Spatio-temporal patterns of topsoil moisture content in a Mediterranean rainfed strip-tilled Almond orchard, Southeast Spain.

Author	D.T.M. Krekel 5874262
Master's program	Bio Inspired Innovation, Utrecht University, Netherlands
Course	General Research Profile - Research project
Examiner	Dr. P.A. Verweij, Utrecht University, Netherlands
Daily supervisor	MSc. C. Bosch, Regeneration Academy, Spain
Publication date	15-03-2024

Utrecht University

Abstract

It is yet unclear how applying 1,5-2 m wide no-till strips in otherwise fully tilled Almond orchards affects the soil's hydrological behaviour. This is a relevant knowledge gap, as in recent years this practise has been applied as a means to regenerate the soil, while keeping the partial benefits of tilling in Mediterranean areas. This led to the research questions: i) *What is the spatial pattern of topsoil moisture content in a Mediterranean rainfed strip-tilled Almond orchard, Southeast Spain?*, ii) *What is the temporal pattern of topsoil moisture content in a Mediterranean rainfed strip-tilled Almond orchard, Southeast Spain?* In this research, dielectric conductivity measurements have been used to as an indication for the spatial and temporal patterns of topsoil moisture content in a rainfed strip-tilled mediterranean almond orchard. Soil compaction testing, point intercept vegetation analysis, soil texture testing, and a Visual Soil Quality assessment all have been performed to give more context to the found patterns. The results showed an increase of measured dielectric conductivity (indication soil moisture) away from the almond trees, peaking however not farthest away from the trees but where topsoil compaction was highest (lowest value 28 mV = 2,6 %vol, highest value 172 mV = 14,0 %vol, estimated permanent wilting point = 17,5 %vol). Farthest away from the trees, values were still higher than closest to the trees. Standard deviation (indicating change of soil moisture over time) was highest at 0,1m (and the opposite 6,9m), and in the 2,0m-4,5m zone away from the trees, also for the control plot. Sensor readings were off due to influence by touch (0,14-2,26 %vol, median ~1,0 %vol). It can be concluded that the topsoil moisture content is lower in the till areas, relative to the no-till areas. This report also includes a proposal on how to determine if a dielectric conductivity sensor gives true values, or whether it's readouts are affected by degree of soil compaction.

Key words; Topsoil moisture content, topsoil water content, TSWC, strip-till, lane-till, dielectric conductivity, Almond, loam, Mediterranean, Southeast Spain, soil compaction, regenerative agriculture.

Layman summary

In this research, it was investigated if and how only partially instead of fully tilling the soil of an almond orchard located in the Mediterranean affects the amount of moisture present in the top 5,1 cm of the soil. Tilling are different ways of mechanically raking the soil to achieve e.g. the removal of weeds, or to improve the infiltration of rainwater. In the researched tilled orchard, there were two-meter-wide strips between each pair of trees where tillage was not practiced. For this research, dielectric conductivity measurements have been performed in the topsoil at several places between pairs of trees. Dielectric conductivity is a physical quantity that can indicate how much moisture is present in the soil. Also, soil compaction (firmness) has been tested at several locations, as was the amount of vegetation covering the soil, soil texture has been determined (the ratio between very small, small, and larger soil particles), and based on visual ques the soil quality was assessed, all to give more context to the dielectric conductivity measurements results. The results showed an increase of measured dielectric conductivity away from the almond trees. However, the values peaked not farthest away from the trees, but there where topsoil compaction was highest. Still, farthest away from the trees values were higher than closest to the trees. There was a significant difference in values between the till and the no-till area. The lowest measured value in the orchard indicated the soil to consist for 2,6% out of water, the highest measured value indicated the soil to consist for 14,0% out of water. For this specific soil it was determined that the permanent wilting point, that is the minimal amount of water that the soil needs to consist out of for a plant to have the chance to grow, was 17,5%. The same locations have been measured three times a week from 01-10-2023 till 26-10-2023 and 15-11-2023 till 08-12-2023. The standard deviation, an indication of how much the values measured at different days at the same location differed, was highest at 0,1m (and the opposite 6,9m), and in the 2,0m-4,5m zone away from the trees. The measured values were thus over time least constant at these locations. During the research it was determined that the readings of the sensor measuring dielectric conductivity were off due to influence by touch, resulting in the sensor indicating the soil to consist out of 0,14 to 2,26 %vol more water than actually is the case, most often the sensor indicated 1 %vol more. All abovementioned measurements have also been performed in a part of the orchard that on purpose has been fully tilled, functioning as a reference. This report also includes a proposal on how to determine if a dielectric conductivity sensor gives true values, or whether its readouts are affected by degree of soil compaction.

Table of Contents

Introduction

Being the second biggest Almond producing country in the world (Social i Company & Gradziel, 2017, p72), Spain has a great objective to adapt their agricultural practices to a changing climatic and environmental context. In the semi-arid regions of the Iberian Peninsula drought periods are predicted to stretch several months longer as was historically and rain events to become more severe in the coming decades (Andrade et al., 2021). Soil erosion is high and soil health low in traditionally wide spaced bare soiled Almond orchards, which likely becomes even more severe under these more sparce and intense rain events (García-Ruiz, 2010). The evoked management transition comes with the help of some governmental financial aid. For 2023-2027 the European Union enforced a new common agricultural policy (CAP), which includes support for agricultural practices that are more sustainable (CAP 2023-27, 2024). As part of CAP farmers in Spain can now receive financial support for implementing spontaneous or sown vegetation coverage (green manure) in tree orchards (MAPA, 2022).

Facilitating vegetation coverage implies no tillage activity in the assigned area. Traditionally tillage is performed with a perceived objective of increasing water absorption (TAFE Corporate, 2022). Unfortunately, this practice also accelerates soil erosion in rainfed tree orchards (García-Ruiz, 2010). Next to that, the soil can lose its natural mechanisms for decompaction, making soils dependent on tillage for infiltration since otherwise crust formation takes place, especially in Mediterranean contexts (Talukder et al., 2022). Also, sped up soil organic matter oxidation eventually can deplete the soil from all organic matter, and the soil biome who naturally fertilize crops might get demolished, leaving the crops dependent on added fertilizers (Lehman et al., 2015). On the other hand, vegetation coverage protects soils from erosion (Raya et al., 2005), seeded or spontaneous ground cover are able to naturally break up the soil with their roots (Zhang & Peng, 2021), and it improves soil moisture content (Ding et al., 2024).

However, in scarce water conditions ground vegetation competes with the crop for moisture negatively affecting yields (Ruíz-Colmenero et al., 2011), creating a dilemma for Spanish farmers. To balance the benefits of both tillage and vegetation coverage, a compromising solution in semi-arid areas could be to integrate the vegetation coverage only partially. Yet, from the perspective of water competition, it is unclear how this would affect the water content pattern in the soil of a tree orchard, specifically with sparsely researched Almond. Because of the recent EU CAP strategy to support vegetation coverage, it is relevant to research soil water content patterns in the context of vegetation strips, as it allows for a more successful implementation of vegetation coverage in semi-arid contexts.

This research gap led to the following objectives; i) to observe the spatial patterns and temporal patterns of topsoil water content in a Mediterranean rainfed strip-tilled Almond orchard, Southeast Spain, while ii) illustrating the context in which these observations are made. The first objective led to the following research questions: i) *What is the spatial pattern*

of topsoil moisture content in a Mediterranean rainfed strip-tilled Almond orchard, Southeast Spain?, ii) *What is the temporal pattern of topsoil moisture content in a Mediterranean rainfed strip-tilled Almond orchard, Southeast Spain?* It is hypothesized that topsoil moisture content increases away from the Almond trees, and, independent from position relative to an Almond tree, is higher in the no-till areas compared to the till areas. It is also hypothesised that there is more temporal difference in topsoil moisture content in the tilled zone compared to the no-till zone.

The research has been performed in a rainfed Almond field located in the Region of Murcia, Spain. The soil has been defined to be a Xerosol (Food and Agriculture Organization of the United Nations, n.d.) and the field is at 450 m altitude with around 420 mm rain a year. In this field three plots of five adjacent Almond tree pairs have been defined, two plots included a 1,5-2 m wide no-till strip, one plot had full tillage. Different types of measurements have been taken along the transects between each tree pair, and parallel to these transects. This report is structured in a Methodology, Results, Conclusion, and Discussion chapter. These chapters will all start describing the topsoil moisture content testing, followed by soil compaction testing, ground cover analysis, tool validation testing, sensor bias testing, and in the Supplements a visual soil quality assessment, the soil texture Jar test, and rainfall monitoring, for context interpretation.

Methodology

General setup

For this research three different research plots have been defined (Figure 1). All of them were located in a rainfed Almond field of a conventional farm turning organic, in the municipality of Moratalla, Region of Murcia, Spain. For reference, the coordinates 38°12'59.9"N 1°49'43.6"W are located within this field, outside the plots. The field was a roughly 25 y.o. Almond field, with trees planted in a 7mx7m grid. The field has historically been conventionally managed, including intensive tilling and artificial input. For 2 years the field has been managed organically, and contains 1,5-2 m wide no-till strips in the middle between each tree row running North to South. The three defined plots in this field consisted all out of five adjacent tree pairs. All plots had roughly similar slopes towards the same direction and were fairly flat without distinct erosion channels.

The imaginary transects between each tree pair were labelled the 'primary' transects, along which measurements for several different experiments documented in this report were taken. These transects were numbered 1 to 5 from North to South. Parallel to these primary transects lay the so called unnumbered 'secondary' transects, along which also measurements were taken. The researcher always moved along the South side of each of the primary transects, to prevent proximate uphill soil disturbance that could influence topsoil moisture content along the transect after a possible rain event. The different experiments that have been performed within this research included topsoil moisture content testing including a control group, soil compaction testing, ground cover analysis, tool validation testing, sensor bias testing, a visual soil quality assessment, the soil texture Jar test, and rainfall monitoring.

The Eastern most plot was labelled 'Main plot' (Figure 2), here primarily topsoil moisture content measurements were taken. The neighbouring plot was labelled 'Shadow plot' and allowed for measurements that complimented the topsoil moisture content measurements but should not interfere with these (e.g. because of causing soil disturbance). The Western most plot was labelled 'Control plot' and was located one tree row more towards the West and one tree pair more towards the North. This was because a full till procedure was eventually performed in this lane, and a tree was missing at the height of the Main and Shadow plot's first primary transect (see Figure 1).

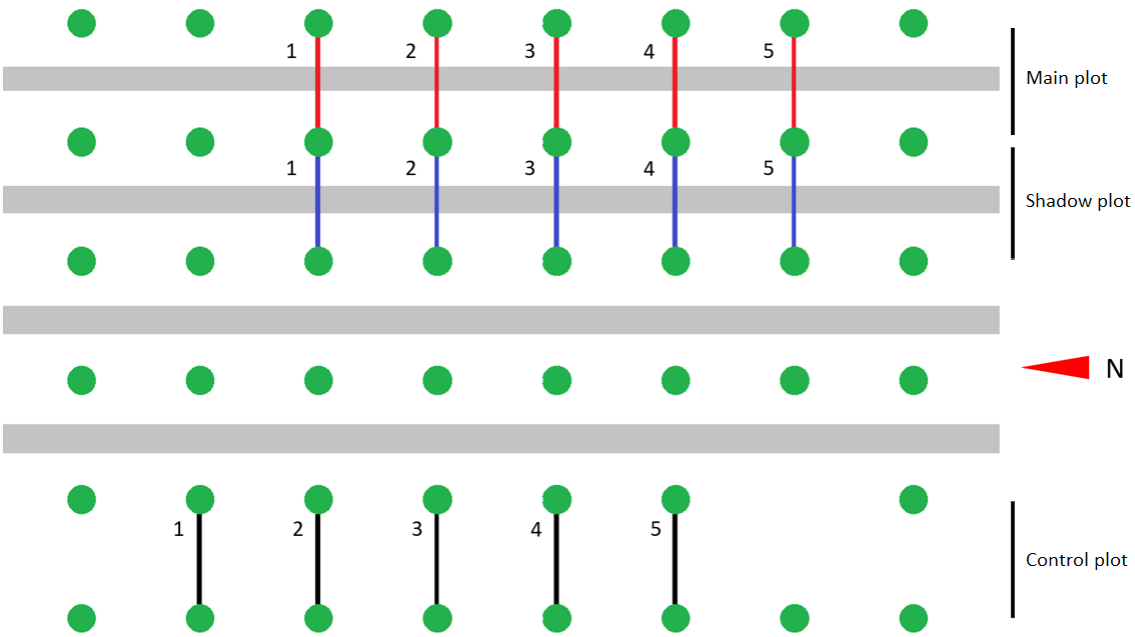

Figure 1. *Overview of research plots and primary transects along which measurements were taken (Red = transects Main plot, Blue = transects Shadow plot, Black = transects Control plot). Green = Almond trees, White = till area, Grey = no-till area.*

Figure 2. *Southwards view on Main plot.*

Topsoil moisture content testing

In the beforementioned 7 m wide Main plot (Figure 1) the moisture content of the top 5,1 cm soil has been spatially and temporally measured using a delta-T SM150t sensor kit. Along the five primary transects of the Main plot measurements were taken every 0,1m, 0,5m, 1,0m, 1,5m, 2,0m, 2,5m, 3,0m, 3,5m, 4,0m, 4,5m, 5,0m, 5,5m, 6,0m, 6,5m, and 6,9m away from the Western tree trunk strip. These measurements were repeated three times a week during the periods 01-10-2023 till 26-10-2023 and 15-11-2023 till 08-12-2023, between 10:00 and 18:00 summertime (times similar to López-Vicente et al., 2015). The rods of the sensor head were pushed vertically into the ground at each observation location, and while still holding the sensor head, a measurement was taken, and the displayed value was noted down. This was repeated three times before moving to the next observation location. The device was set to display the measured dielectric conductivity expressed in mV. Halfway through the first measuring period observation location determination switched from being done using a 3 m measuring tape to using a 7 m measuring rope, with indications every 0,5m and at 0,1m and 6,9m. During the second measuring period only the measuring rope has been used. Also, no more measurements have been taken at locations 2,5m and 4,0m/4,5m for each of the transects during the second measuring period in order to spare the equipment due to high soil compaction. Therefore the data from these two measuring periods were analysed separately in all the belowmentioned analyses.

Based on the obtained results, the Mean Relative Difference (MRD) and the Standard Deviation of the Relative Difference (SDRD) have been calculated based on equations 2 to 4 from the report of López-Vicente et al. (2015) (see equation 1 to 3 in this report). However, in this research dielectric conductivity instead of volumetric moisture content has been used as a value for θ. The MRD indicates a spatial dielectric conductivity value pattern by showing the relative difference of the average measured values at each observation location against the average measured values of the whole field, taking all the measurements of all measuring days. The SDRD shows a temporal dielectric conductivity value pattern by showing at which observation locations there is more and at which there is less variance in the measured dielectric conductivity values, taking again all the measurements of all measuring days relative to the field average. Higher variance in measured dielectric conductivity values at a single observation location assumes a more instable topsoil moisture content. The equations calculate "the relative difference, δ_{it}, between the average value of θ_0 in the whole study area at the time or survey "*t*", θ_{0t}, and the specific value of θ_0 at each observation location "*i*", where MRD_i is the mean relative difference for the location "*i*" and *NT* is the number of observation times. And the temporal stability analysis of these differences was done calculating the standard deviation of the set $\delta_{i,1}, \delta_{i,2}, \ldots, \delta_{i,NT}$ of relative differences at the location "*i*" over the […] field surveys:" (López-Vicente et al., 2015).

(1) $$\delta_{it} = \frac{\theta_{0it} - \overline{\theta_{0t}}}{\overline{\theta_{0t}}}$$

(2) $$MRD_i = \frac{1}{N_T}\sum_{t=1}^{t=N_T}\delta_{it}$$

(3) $$SDRD_i = \sqrt{\frac{1}{N_T - 1}\sum_{t=1}^{t=N_T}(\delta_{it} - MRD_i)^2}$$

The same methodology has been used to measure the topsoil moisture content along the primary transects of the Control plot at the dates 29-11-2023, 30-11-2023, 14-12-2023, (transects 4 (incomplete) and 5), and 16-12-2023 (of which transect 5 incomplete), also between 10:00 and 18:00. For the Main plot measurements at 06-12-2023, 08-12-2023, and 10-12-2023 and the Control plot measurements at 14-12-2023 and 16-12-2023 before each measurement an extra measurement was taken whereby the sensor head was not held, between these measurements the sensor was not removed out of the soil. Further in the report this will be referred to as "Sensor bias testing". For the Sensor bias testing these obtained sensor values denoting the dielectric conductivity in mV were then converted to the soil refractive index ($\sqrt{\varepsilon}$) and subsequently to volumetric soil moisture content (θ), using equations 4 and 5 with the Mineral soil constants a0 = 1,6 and a1 = 8,4 (Delta-T Devices Ltd, 2016, p. 20) based on a carbon content of 0,607 % Fitosoil Laboratorios, S.L., 2022). Subsequently for each double measurement the difference between these two values have been calculated.

(4) $\sqrt{\varepsilon} = 1+14{,}4396*V-31{,}2587*V^2+49{,}0575*V^3-36{,}5575*V^4 +10{,}7117*V^5$

(5) $\theta = (\sqrt{\varepsilon}-a0)/a1$

To follow up on the obtained MRD pattern, further statistical analysis has been performed to determine whether there is a significant difference in measured dielectric conductivity values between each location, this time grouping all the transects together. All measured dielectric conductivity values at one location (e.g. 1,5m) from all transects and each measuring day were considered a single group. With group sizes between 170 and 180 the groups were large enough for statistical analysis as a group size of 64 was required (effects 0,5, *p*-value 0,05, power 0,8), only for the Control plot group sizes were often below 64. To determine if the obtained SDRD values represent significant differences in variance between the groups, a Levene's test and Tukey HSD post-hoc test have been performed on the same groups of values as for the SDRD calculations.

Soil compaction testing

Soil compaction has been tested using an Agratronix Soil Compaction Tester, also known as a penetrometer, using the accessory small tip with a diameter of ½" (1,27 cm). The shaft of the instrument has marks every 3 inches with which penetration depth has been determined. To take a measurement, the penetrometer has been held with two hands, by a person weighting 56 kg, and vertically pressed down into the soil. For both the Main plot and Shadow plot it has been noted down at which depth the penetrometer could not be pushed further into the soil using full body weight to push. For the Shadow plot it has also been noted down starting at which depth more than 200 psi (pounds per square inch) and more than 300 psi were necessary to enable soil penetration.

Soil compaction has been tested in 2 of the 3 aforementioned plots, the Main plot (10-12-2023) and the Shadow plot (19-11-2023). In both plots soil compaction has been tested along imaginary secondary transects laying parallel to the aforementioned primary transects (see Figure 1) between each of the plot's 5 tree pairs. For the Main plot these secondary transects ran parallel 1 meter Southwards to the primary transects. Along these secondary transects soil compaction has been measured at 0,1m, 0,5m, 1,0m, 1,5m, 2,0m, 2,5m, 3,0m, 3,5m, 4,0m, 4,5m, 5,0m, 5,5m, 6,0m, 6,5m, and 6,9m away from the plot's Western tree trunk line (Figure 3). For the Shadow plot these secondary transects ran parallel 1,5 meter Southwards to the primary transects and soil compaction has been measured at 0,1m, 0,5m, 1,0m, 1,5m, 2,0m, 2,5m, 3,0m, 3,5m, 4,0m, 4,5m, 5,0m, 5,5m, 6,0m, and 6,4m away from the plot's Western tree trunk line.

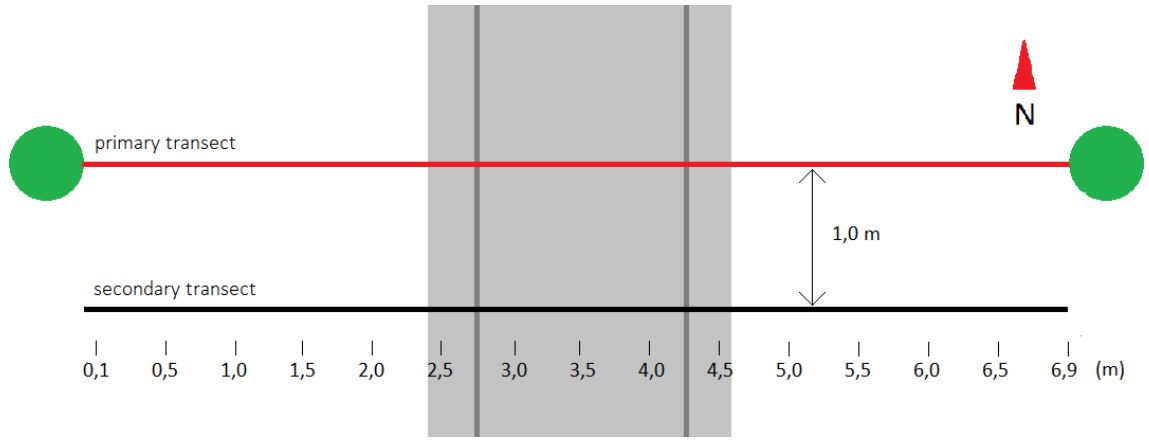

Figure 3. *Locations of soil compaction testing points in the Main plot along one of the plot's five secondary transects.*

Due to the crude depth measurement scale, values were estimated, rounded off, and only noted down in steps of 1/5th of 3", 1/3th of 3", or ½th of 3". As this report is written using the metric system, the values in the imperial system unit inches have been converted to cm using 1" = 2,54 cm. For data interpretation, the crudeness of the values has been taken into account. After soil compaction testing, an asana has been used to scrape off uncompacted soil, therefore exposing a first layer of compacted soil. This has been done at the second secondary transect in the Main plot, between 0,5m and 2,0m away from the Western tree trunk line.

Ground cover analysis

Ground coverage has been determined by analysing ground surface images using the software program 'SamplePoint' (Booth et al., 2006) which enables point intercept analysis (Drezner & Drezner, 2021). The ground surface images have been taken on several different days in October and November 2023 using a Samsung A405FN smartphone (F1,7, ISO 40, White balance AUTO, no flash), using a nadir angle at roughly 1,5m height. The areas that have been photographed were slightly Northwards from the Eastern till regions and the no-till regions of the Main plot primary transects (to exclude due to other experiments disturbed soil

from the images), and overlayed the Eastern till regions and the no-till regions of the Shadow plot primary transects (Figure 4). The images display measuring tape and measuring rope that have been used to determine the correct photographing location in the field. Images were cut to ensure that no tree line areas or tire tracks were included.

These processed images were then uploaded into 'SamplePoint' and point intercept analysis has been performed using the '15x15 = 225' grid size option. As no present vegetation showed a filled canopy it was assumed that the largest amount of grid points could be used without a deterioration in accuracy, and should be used to ensure highest possible precision (Drezner & Drezner, 2021). With a grid of 225 sampling points and the estimated largest vegetation diameter relative to the eventual grid points spacing it is assumed that the obtained values have a less than 2% expected deviation from reality (see Figure 2C in Drezner & Drezner, 2021). Labels that have been used to characterise the sample points were Tumbleweed (Tumbleweed, most likely *Kali Tragus*), Plant (Living plant, other than Tumbleweed), Litter (Organic litter), Soil (Bare soil or stone), Equipment (Research equipment: measuring tape or measuring rope), and Unknown (Uncharacterised pixel). Obtained point intercept ground cover analysis observation values were averaged for each plot and till regime zone and converted to percentages. The observations labelled as 'Equipment' were left out of the result analysis.

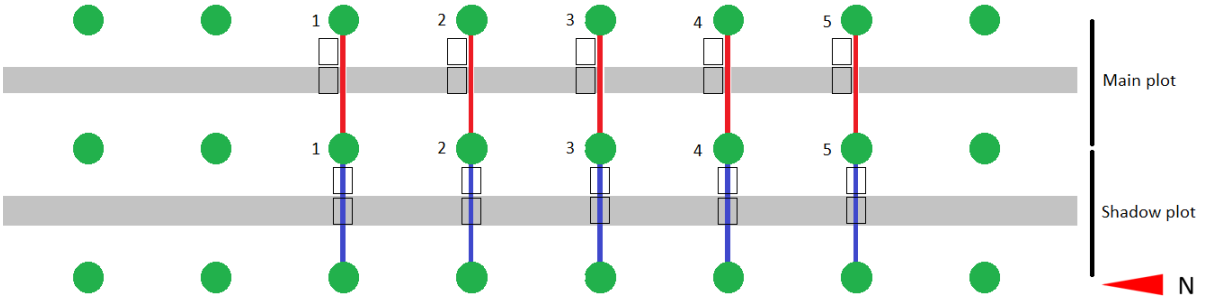

Figure 4. *Black squares indicate areas of which nadir images have been taken that were analysed using the 'SamplePoint' software program. Green = Almond trees, White = till area, Grey = no-till area, Red = transects Main plot, Blue = transects Shadow plot.*

Tool validation

HEMA felt tip pens have been used to determine observation zones (Figure 5). Along transects 1, 2, and 3 from the Shadow plot these pens have been placed with their middle at 0,1m, 1,5m, 2,5m, 3,0m, 3,5m, 4,25m, 5,0m, and 6,4m (two observation zones near Almond trees, full in the till zone, on the tire tracks, and full in the no-till zone) away from the plot's Western tree trunk line. The size of the pens determined an imaginary square observation zone at the Northside of the transect/pen, with the pen forming the lower base of the square.

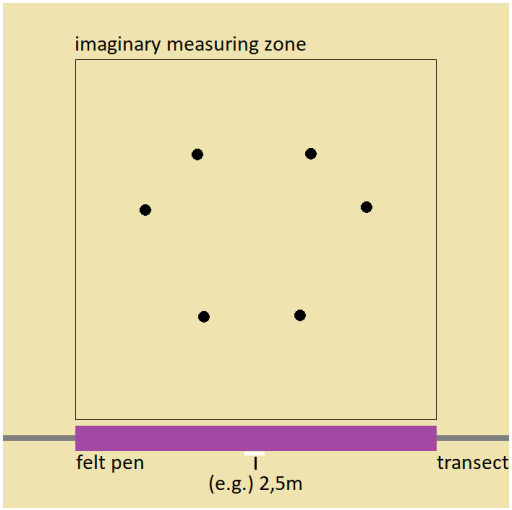

Figure 5. *Soil measuring zone (black square) indicated by felt pen (purple) placement along transect (grey). Dots indicate measuring points for bi-pin dielectric conductivity sensor.*

Per observation zone three soil dielectric conductivity measurements have been taken, using the SM150t sensor kit. Measurement points were positioned in a triangle formation within the square whenever possible. The rods of the sensor head were pushed vertically into the ground at each measuring point, and while still holding the sensor head, a measurement was taken, and the displayed value was noted down. The device was set to display the measured dielectric conductivity expressed in mV. This is similar to the Topsoil moisture content testing protocol described before, however measurements were not repeated. Next, from each zone a 200g-350g soil sample has been taken, including soil only from the top 7 cm layer. The soil samples were then sieved using a kitchen sieve and transferred to a up to 480 °C heat resistant microwave resistant glass bowl of which the weight was known at 0,01 g precision. The combined weight of each soil sample and glass bowl were noted down. For each soil sample the sample and glass bowl were then placed in a microwave in which the sample was heated up for 1 minute at 500 W, a reliable method with results comparable to air oven drying (Prokopowicz et al., 2020). After this soil temperature was measured using an Infrared Thermometer Surpeer IR5D Laser and the sample and bowl were weighted using a precision scale. This process was repeated until the weight difference between each heating step was less than 0,05 g or even negative, thus taking into account the empirically noted inaccuracy of the precision scale. Per observation zone the average soil dielectric conductivity measurement values were set out against Δweight of the soil sample, on which a regression analysis and Cook's Distance test have been performed.

This experiment has been performed in December 2023. Soil samples from transect 1 locations 0,1m-2,5m have been microwave dried at the day of dielectric conductivity measuring and sample taking, soil samples from transect 1 locations 3,0m-6,4m have been microwave dried one day after. Soil samples from transect 2 locations 0,1-3,0m have been microwave dried two days after dielectric conductivity measuring and sample taking, soil samples from transect 2 locations 3,5-6,4m have been microwave dried three days after dielectric conductivity measuring and sample taking. Soil samples taken at transect 3 were stored too long, and could not be used anymore. Transects 1 and 2 have not been sampled at the same day.

Visual Soil Assessment

A Visual Soil Assessment (VSA) has been performed in the Shadow plot following the methodology described by Soto et al. (2020) (see Soto et al., 2020 Supplement A). This VSA determines the quality of the soil by assessing different soil quality related characteristics, being; soil structure, soil organic matter content, root abundance, worm abundance, soil humidity, soil temperature, vegetation cover, ground cover vegetation colour, presence of vegetation types, degree of erosion, infiltration capacity, yield size and quality, crop vigour, and presence of ladybugs and other insects. The VSA refers to visual cues by which each characteristic can be scored to be of low, medium or high quality, totalling up to an overall indication of low, medium or high soil quality. This methodology has been developed in the region where the research field is located. Assessment questions 8, 12.1, and 13 have not been answered, as the assessment has been performed in the Autumn.

Soil texture test

To determine the soil texture of the field's soil, a "Jar test" has been performed following the protocol by Jeffers (2019). According to the protocol, a jar was filled about 1/3 with soil, a tablespoon of powdered clothes washing detergent was added, the jar was filled up with water, after which the jar was firmly shaken. Once the jar was placed still on a table, the hight of the sedimentation was measured after 1 minute, 2 hours, and 24 hours. The used soil sample was taken from the top 10 cm soil of an area next to the Main plot, inside the field, outside the research plots. The Jeffers (2019) protocol speaks of powdered dishwashing detergent, here instead powdered clothes washing detergent was used. The sedimentation after 1 minute was supposed to indicate the sand fraction, sedimentation between 1 minute and 30 minutes to indicate the silt fraction, and sedimentation between 30 minutes and 24 hours to indicate the clay fraction.

Known soil particle ratios then allowed for permanent wilting point estimations using the Briggs and Shantz (1912) wilting coefficient equation (6). This equation is used as an estimation, as no soil matric potential measurements could be performed. The permanent wilting point is known to depend on more than soil texture alone (Kirkham, 2005).

(6) $Wilting\ coefficient = 0{,}01\ sand + 0{,}12\ silt + 0{,}57\ clay$

Rainfall monitoring

From 09-09-2023 till 17-12-2023 a pluviometer was placed at 38°13'12.0"N 1°49'06.5"W. As soon as possible after each rain event the water level was read from the pluviometer after which the pluviometer was emptied and repositioned. Quick readout was done to prevent anticipated evaporation of caught rainwater.

Results

Topsoil moisture content testing

The analysis of topsoil moisture content is described below in several steps. For the analysis the obtained measurement data has been ordered in three different datasets: Main plot period 01-10-2023 till 26-10-2023, Main plot period 15-11-2023 till 08-12-2023, and Control plot. First, is analysed how the different individual observation locations differ in measured dielectric conductivity values, under section “Spatial analysis: Mean relative difference”. Secondly, is analysed how the different individual observation locations differ in the degree of change in measured dielectric conductivity values, under section “Spatial analysis: Standard Deviation of the Relative Difference”. After this, statistical analysis is performed to determine whether specific observation locations fall into statistically differentiable zones based on measured dielectric conductivity values, under sections “Statistical analysis: […] dataset”. To enable this analysis, measurements for all transects were merged together per dataset. To conclude, statistical analysis is performed to determine if there is a significant change in measured dielectric conductivity values between locations and in general between measuring days, under section “Statistical analysis: Difference in variance between measuring days”.

Spatial analysis: Mean relative difference

To show a possible increase or decrease of topsoil moisture content away from the almond trees the mean relative difference has been calculated. The Mean Relative Difference between point value and field average of all readout values from each measuring day taken together in Main plot dielectric conductivity measurements dataset 01-10-2023 till 26-10-2023 and dataset 15-11-2023 till 08-12-2023 are shown in Figure 6 and Figure 7. The Mean Relative Difference between point value and field average in the Control plot are shown in Figure 8. A Pearson correlation analysis between the Mean relative difference data of the Main plot dielectric conductivity measurements dataset 01-10-2023 till 26-10-2023 (Figure 6) and the Control plot dataset (Figure 8) shows a significant high positive correlation (r = 0,75, p-value < 0,001). Lowest and highest dielectric conductivity readouts in the Main plot dielectric conductivity measurements dataset 01-10-2023 till 26-10-2023 were 28 mV and 172 mV. This corresponds to a derived lowest and highest topsoil moisture content value of -2,6 %vol and 14,0 %vol, which is below the actual possible lowest topsoil moisture content value of 0,0%.

	0,1	0,5	1	1,5	2	2,5	3	3,5	4	4,5	5	5,5	6	6,5	6,9
tr 1	-0,71838	-0,62506	-0,29220	-0,18109	0,06861	1,24658	0,72408	0,30209	1,10426	0,52772	0,38632	-0,00833	-0,07881	-0,47742	-1,00764
tr 2	-0,85494	-0,58583	-0,32991	0,18012	0,00838	1,21529	0,56443	0,43542	0,65801	1,08816	0,09835	-0,30959	-0,25512	-0,45212	-0,75336
tr 3	-0,28552	-0,19740	-0,24071	-0,09196	-0,01349	1,25695	0,53807	0,67245	1,20952	0,66184	-0,23428	-0,33748	-0,22863	-0,51246	-0,71070
tr 4	-0,55468	-0,57079	-0,36152	-0,33413	-0,17904	0,41589	0,28272	0,28582	0,89320	0,73261	0,02863	0,03987	-0,49419	-0,86401	-1,18811
tr 5	-0,78623	-0,41310	-0,22458	-0,19836	0,16989	0,66337	0,09889	0,36481	0,73096	0,67739	-0,24813	-0,29903	-0,41232	-0,59656	-0,45573

Figure 6. *Mean Relative Difference between point value and field average (4,22425) of all readout values from each measuring day taken together in Main plot dielectric conductivity measurements dataset 01-10-2023 till 26-10-2023, including colour scale from red (negative value) to green (positive value).*

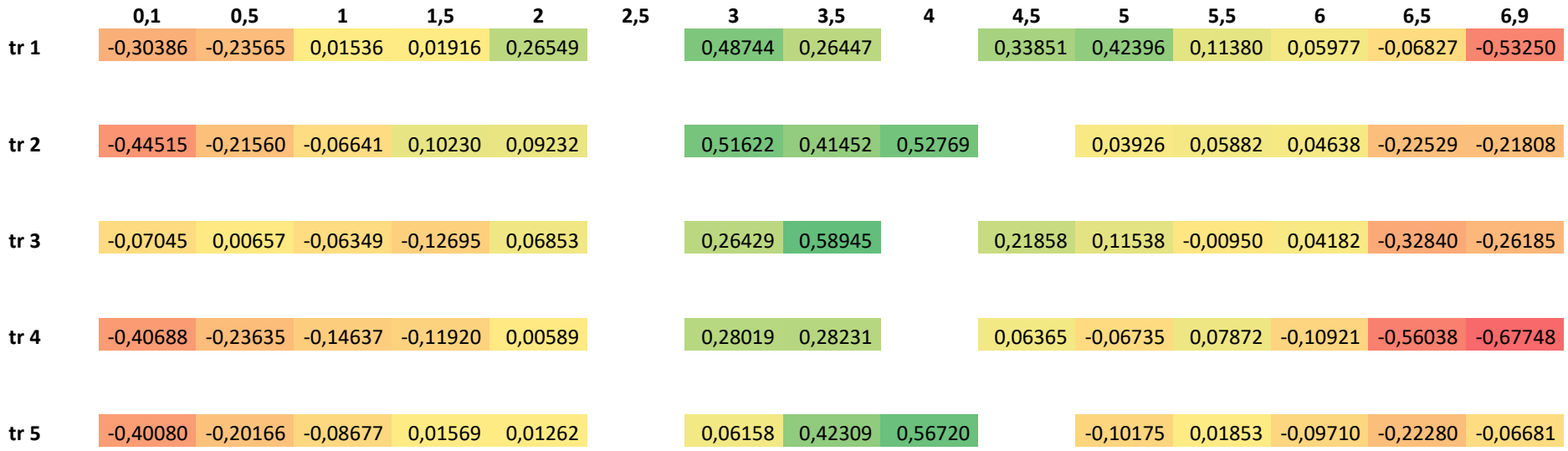

	0,1	0,5	1	1,5	2	2,5	3	3,5	4	4,5	5	5,5	6	6,5	6,9
tr 1	-0,30386	-0,23565	0,01536	0,01916	0,26549		0,48744	0,26447		0,33851	0,42396	0,11380	0,05977	-0,06827	-0,53250
tr 2	-0,44515	-0,21560	-0,06641	0,10230	0,09232		0,51622	0,41452	0,52769		0,03926	0,05882	0,04638	-0,22529	-0,21808
tr 3	-0,07045	0,00657	-0,06349	-0,12695	0,06853		0,26429	0,58945		0,21858	0,11538	-0,00950	0,04182	-0,32840	-0,26185
tr 4	-0,40688	-0,23635	-0,14637	-0,11920	0,00589		0,28019	0,28231		0,06365	-0,06735	0,07872	-0,10921	-0,56038	-0,67748
tr 5	-0,40080	-0,20166	-0,08677	0,01569	0,01262		0,06158	0,42309	0,56720		-0,10175	0,01853	-0,09710	-0,22280	-0,06681

Figure 7. *Mean Relative Difference between point value and field average (4,09937) of all readout values from each measuring day taken together in Main plot dielectric conductivity measurements dataset 15-11-2023 till 08-12-2023, including colour scale from red (negative value) to green (positive value). Gaps indicate locations where no measurements were taken to prevent sensor damage due to high soil compaction.*

	0,1	0,5	1	1,5	2	2,5	3	3,5	4	4,5	5	5,5	6	6,5	6,9
tr 1	-1,08684	-0,66417	-0,04018	0,12738	0,09058	0,41287	0,92892	0,48061	0,39711	0,20143	0,23074	0,46662	0,21305	-0,33852	-0,81542
tr 2	-0,55043	-0,69054	0,05758	-0,01577	0,78802	0,65756	0,77085	-0,06851	0,53750	-0,21740	0,12441	0,14705	-0,02132	-0,81223	-0,62306
tr 3	-0,70248	-0,43360	-0,09494	0,01792	0,45333	0,75843	0,58990	0,31841	0,60617	-0,05442	-0,01430	0,20017	0,29035	-0,54012	-0,97663
tr 4	-0,99900	-0,28674	0,04935	-0,13862	0,05235	0,39747	0,43061	0,06392	0,62945	0,22368	0,15536	0,33391	0,21725	-0,29161	-1,17512
tr 5	-0,93184	-0,45788	-0,16817	0,02545	0,23567	0,30945	0,53433	0,14064	0,31818	0,18505	0,04841	0,40460	-0,03821	-0,67227	-0,69506

Figure 8. *Mean Relative Difference between point value and field average (2,67686) of all readout values from each measuring day taken together in Control plot dielectric conductivity measurements dataset, including colour scale from red (negative value) to green (positive value).*

Temporal analysis: Standard deviation of the Relative Difference

To show a possible change of topsoil moisture content over time at each measurement location the Standard Deviation of the Relative Difference (SDRD) has been calculated. SDRD of all readout values from each measuring day taken together in Main plot dielectric conductivity measurements dataset 01-10-2023 till 26-10-2023 and dataset 15-11-2023 till 08-12-2023 are shown in Figure 9 and Figure 10. SDRD of the Control plot are shown in Figure 11. A Pearson correlation analysis between the SDRD data of the Main plot dielectric conductivity measurements dataset 01-10-2023 till 26-10-2023 (Figure 10) and the Control plot dataset (Figure 11) shows a significant low positive correlation (r = 0,46, p-value < 0,001), indicating that the found SDRD patterns between the Main plot measurements and the Control plot measurements are not very dissimilar.

	0,1	0,5	1	1,5	2	2,5	3	3,5	4	4,5	5	5,5	6	6,5	6,9
tr 1	0,52327	0,50506	0,24076	0,22960	0,15619	0,24710	0,34870	0,41970	0,36359	0,49076	0,69362	0,38260	0,26786	0,23827	0,36232
tr 2	0,45415	0,22153	0,13913	0,55667	0,33041	0,94456	0,41851	0,20649	0,42058	0,44962	0,30728	0,40914	0,37605	0,47663	0,49153
tr 3	0,57510	0,32059	0,12476	0,23429	0,34720	0,69123	0,47558	0,36054	0,58179	0,43438	0,13048	0,17119	0,22232	0,30263	0,44192
tr 4	0,57934	0,59617	0,37760	0,34899	0,18701	0,43439	0,29529	0,29853	0,93292	0,76518	0,02991	0,04164	0,51617	0,90242	1,24094
tr 5	0,82119	0,43146	0,23456	0,20719	0,17745	0,69287	0,10329	0,38103	0,76346	0,70751	0,25916	0,31232	0,43066	0,62309	0,47599

Figure 9. *Standard Deviation of the Relative Difference between point value and field average (4,22425) of all readout values from each measuring day taken together in Main plot dielectric conductivity measurements dataset 01-10-2023 till 26-10-2023, including colour scale from green (lower values) to red (higher values).*

	0,1	0,5	1	1,5	2	2,5	3	3,5	4	4,5	5	5,5	6	6,5	6,9
tr 1	0,27293	0,21216	0,15137	0,10571	0,14646		0,14851	0,16165		0,15536	0,20320	0,11205	0,15674	0,14227	0,11392
tr 2	0,18311	0,09581	0,06118	0,08512	0,10700		0,15081	0,12081	0,13145		0,17255	0,10343	0,13968	0,19988	0,12135
tr 3	0,16601	0,10539	0,07088	0,21867	0,10371		0,08346	0,15220			0,11159	0,10732	0,06450	0,09134	0,11916
tr 4	0,13217	0,14261	0,16485	0,16714	0,19038		0,20628	0,21724		0,21670	0,21968	0,18248	0,14341	0,11267	0,09369
tr 5	0,11139	0,07741	0,11683	0,24568	0,22433		0,10942	0,12621	0,24857		0,08985	0,12383	0,07884	0,10053	0,12636

Figure 10. *Standard Deviation of the Relative Difference between point value and field average (4,09937) of all readout values from each measuring day taken together in Main plot dielectric conductivity measurements dataset 15-11-2023 till 08-12-2023, including colour scale from green (lower values) to red (higher values).*

	0,1	0,5	1	1,5	2	2,5	3	3,5	4	4,5	5	5,5	6	6,5	6,9
tr 1	1,88247	1,15037	0,06959	0,22062	0,15689	0,71512	1,60894	0,83244	0,68782	0,34889	0,39966	0,80821	0,36902	0,58634	1,41235
tr 2	0,95338	1,19606	0,09972	0,02731	1,36489	1,13893	1,33515	0,11866	0,93098	0,37655	0,21548	0,25470	0,03693	1,40682	1,07918
tr 3	1,21672	0,75101	0,16444	0,03104	0,78519	1,31363	1,02173	0,55151	1,04991	0,09426	0,02476	0,34670	0,50291	0,93551	1,69157
tr 4	1,99800	0,57347	0,09870	0,27724	0,10471	0,79495	0,86121	0,12784	1,25890	0,44735	0,31072	0,66781	0,37630	0,50509	2,03537
tr 5	1,86368	0,79307	0,29128	0,04408	0,40820	0,53598	0,92549	0,24359	0,55110	0,32051	0,08385	0,70078	0,06618	1,16440	1,20389

Figure 11. *Standard Deviation of the Relative Difference between point value and field average (2,67686) of all readout values from each measuring day taken together in Control plot dielectric conductivity measurements dataset, including colour scale from green (lower values) to red (higher values).*

Statistical analysis: Main plot dataset of 01-10-2023 till 26-10-2023

To determine which measurement locations differ significantly in topsoil moisture content, statistical analysis has been performed. This has been done on the Main plot dielectric conductivity measurements datasets of 01-10-2023 till 26-10-2023 and 15-11-2023 till 08-12-2023 and the Control group dataset. In Figure 12 the spread of measured dielectric conductivity values per location in the Main plot during the period 01-10-2023 till 26-10-2023 are visualised. For statistical analysis, all values measured in the Main plot at similar distance away from the Western tree line are considered a group, independent from the day on which the measurement was taken or along which primary transect.

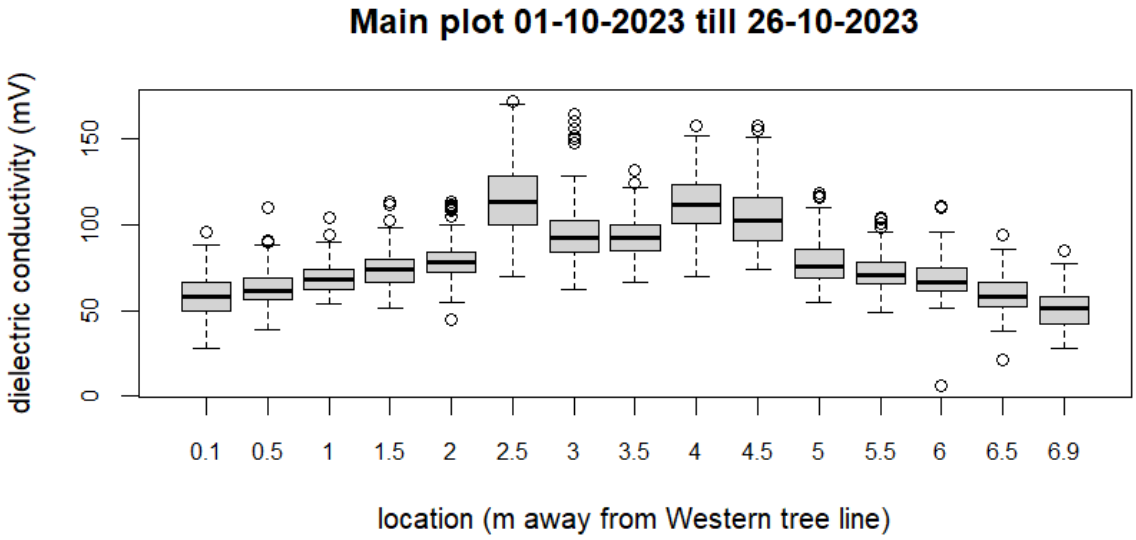

Figure 12. *Dielectric conductivity readings in the Main plot during the period 01-10-2023 till 26-10-2023 along each of the five primary transects.*

The goal was to compare the groups, by comparing the means of the measured values at each location. ANOVA assumes normality and homoscedasticity in the dataset. For this dataset both the hypothesis of normality and homoscedasticity were rejected. The Shapiro-Wilk test for normality showed that the regression residuals derived from the dataset differed from normality (W = 0,97363, *p*-value < 2,2e-16) as is also visible in the residuals QQ plot (Figure 13.a). The Levene's test for homoscedasticity showed that the residuals do not have equal variance between the groups (F(14,2678)=20,9, *p*-value < 2,2e-16), as can also be seen when plotting the residuals against the fitted values (Figure 13.b).

In this case the non-parametric Kruskal-Wallis test can be used to compare the medians between groups. This test requires equal distribution between groups, which is as mentioned not the case (Figure 12). However, the sample size is relatively large (177-180 value points per group). Therefore, the Kruskal-Wallis test will still be used (Ramsey, 1980), while keeping in mind the violation of this assumption. This test shows that there are significant differences between the groups (Chi-squared = 168,92, df = 133, *p*-value = 0,0192). A pairwise Wilcoxon rank sum test with a Benjamini & Hochberg (1995) adjusted *p*-value shows that groups

between which there is no significant difference (thus p > 0,05) are 0,1m-0,5m, 0,1m-6,5m, 0,1m-6,9m, 0,5m-6,5m, 1,0m-1,5m, 1,0m-5,5m, 1,0-6,0m, 1,5m-2,0m, 1,5m-5,0m, 1,5m-5,5m, 1,5m-6,0m, 2,0m-5,0m, 2,5m-4,0m, 2,5m-4,5m, 3,0m-3,5m, 4,0m-4,5m, 5,0m-5,5m, 5,5m-6,0m. Visual analysis shows that these results allow for a grouping into zones, when arrows that point to the same cells are clustered together (Figure 14). These zones form an almost mirrored image away from the Western and Eastern trunk line towards the middle.

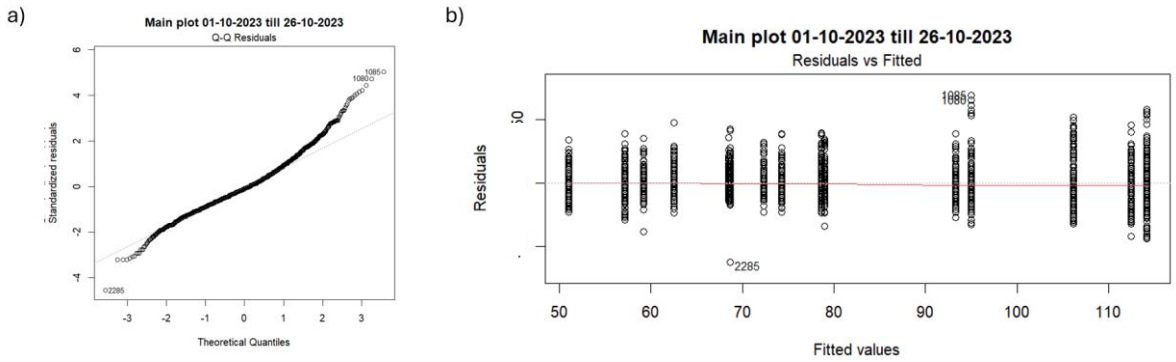

Figure 13.

a) QQ plot of the regression residuals from the Main plot dielectric conductivity measurements dataset of 01-10-2023 till 26-10-2023.

b) Regression residuals plotted against the fitted values for the Main plot dielectric conductivity measurements dataset of 01-10-2023 till 26-10-2023.

a)

groups	0,1m	0,5m	1,0m	1,5m	2,0m	2,5m	3,0m	3,5m	4,0m	4,5m	5,0m	5,5m	6,0m	6,5m	6,9m
0,5m	1,18E+02	NA	NA	NA	NA	NA	NA	NA	NA	NA	NA	NA	NA	NA	NA
1,0m	8,09E-13	1,40E-04	NA	NA	NA	NA	NA	NA	NA	NA	NA	NA	NA	NA	NA
1,5m	5,39E-24	1,00E-15	7,71E-02	NA	NA	NA	NA	NA	NA	NA	NA	NA	NA	NA	NA
2,0m	1,17E-33	2,15E-26	1,28E-14	4,16E+01	NA	NA	NA	NA	NA	NA	NA	NA	NA	NA	NA
2,5m	3,70E-51	6,67E-50	1,04E-48	2,03E-42	1,83E-36	NA	NA	NA	NA	NA	NA	NA	NA	NA	NA
3,0m	1,04E-48	1,75E-45	1,08E-42	6,04E-28	6,40E-17	1,13E-12	NA	NA	NA	NA	NA	NA	NA	NA	NA
3,5m	4,41E-50	2,01E-47	6,66E-46	2,20E-31	3,78E-20	1,31E-16	7,65E+05	NA	NA	NA	NA	NA	NA	NA	NA
4,0m	2,74E-52	9,78E-52	9,78E-52	9,19E-48	5,01E-43	4,62E+05	1,10E-15	1,59E-20	NA	NA	NA	NA	NA	NA	NA
4,5m	1,21E-51	3,11E-50	4,84E-50	1,28E-41	1,87E-33	8,20E+01	2,56E-02	1,83E-04	6,98E+01	NA	NA	NA	NA	NA	NA
5,0m	3,33E-30	1,14E-22	7,37E-09	4,57E+03	3,50E+05	7,93E-36	1,94E-15	3,04E-17	6,21E-41	9,65E-31	NA	NA	NA	NA	NA
5,5m	9,98E-20	3,02E-11	5,42E+02	6,07E+04	4,99E-03	9,84E-45	4,95E-32	4,08E-35	3,26E-49	4,10E-44	5,83E+00	NA	NA	NA	NA
6,0m	1,34E-10	1,19E-02	6,58E+05	7,18E-01	8,58E-11	1,11E-46	2,18E-37	3,08E-40	4,41E-50	1,68E-46	3,03E-07	5,72E+02	NA	NA	NA
6,5m	1,50E+05	9,88E+03	1,11E-10	4,40E-22	4,87E-32	5,99E-51	2,46E-48	5,88E-50	2,85E-52	1,50E-51	1,03E-28	1,27E-17	4,06E-08	NA	NA
6,9m	4,37E+00	3,65E-13	2,32E-32	5,91E-40	2,06E-45	2,85E-52	5,92E-52	2,74E-52	2,74E-52	2,74E-52	1,14E-43	6,17E-37	3,09E-29	1,24E-04	NA

b)

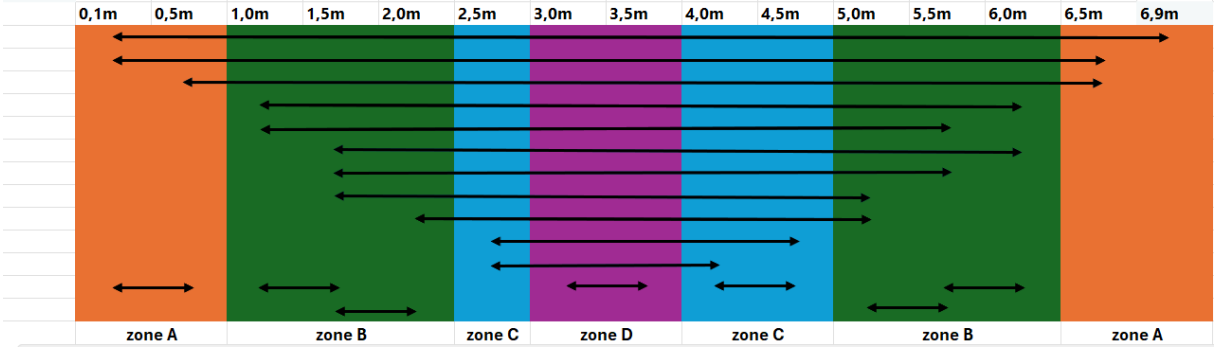

Figure 14. *Visual analysis of the Wilcoxon rank sum test results on the Main plot dielectric conductivity dataset of 01-10-2023 till 26-10-2023.*
a) Green cells show significant test results ($p < 0,05$), white cells show no significant test results.
b) Arrows show between which groups of values there is no significant difference (thus $p > 0,05$).
Coloured planes visualise a suggested grouping into zones.

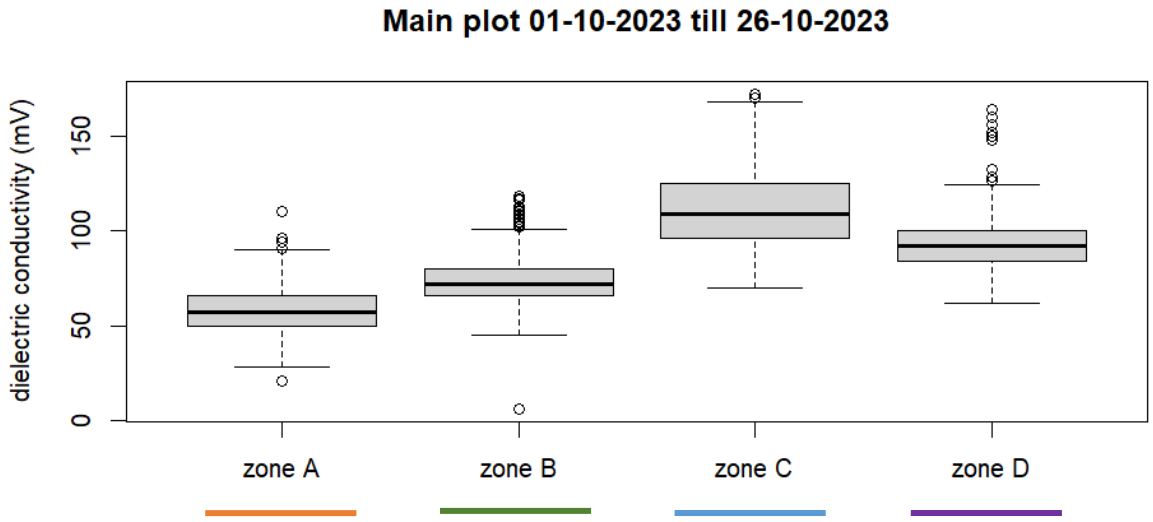

Figure 15. *Dielectric conductivity readings in the Main plot during the period 01-10-2023 till 26-10-2023 along each of the five primary transects. Grouping according to zones defined in Figure 14.*

Statistical analysis have been performed to analyse the data grouped as defined in Figure 14. The Shapiro-Wilk test for normality (W = 0,97751, *p*-value < 2,2e-16) and Levene's test for homoscedasticity (F(3,2689)=73,9, *p*-value < 2,2e-16), indicated non-normality and heteroscedasticity. Consequently a pairwise Wilcoxon rank-sum test has been performed. The test results showed that each group differed significantly.

Statistical analysis: Main plot dataset of 15-11-2023 till 08-12-2023

Similar analyses were done for the dielectric conductivity measurements performed in the Main plot during the period 15-11-2023 till 08-12-2023 (Figure 16) and measurements performed in the Control plot (Figure 20).

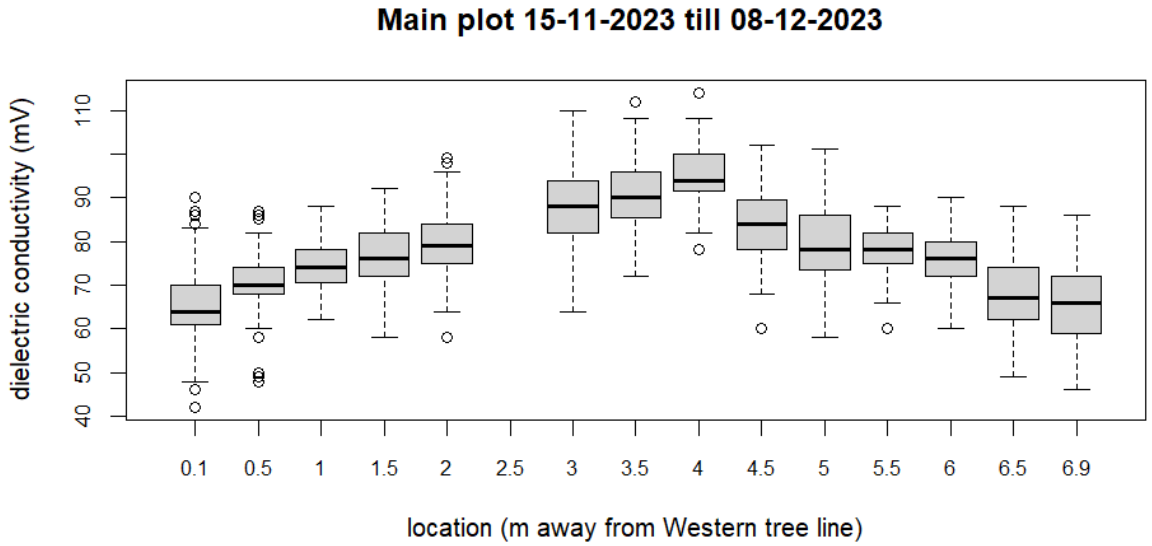

Figure 16. *Dielectric conductivity readings in the Main plot during the period 15-11-2023 till 08-12-2023 along each of the five primary transects. No data at location 2,5m.*

For the Main plot data period 15-11-2023 till 08-12-2023 the Shapiro-Wilk test could not detect non-normality (W = 0,99891, *p*-value = 0,1221) in the regression residuals derived from the dataset. The residuals QQ plot for this dataset indicates normality (Figure 17.a). Therefore, the first assumption for ANOVA is met. However, the Levene's test indicates no equal residues variance between the groups ($F(13,2473) = 12,2$, *p*-value = 3,98e-26), as is also visible in Figure 17.b. Therefore, the second assumption of ANOVA is violated. Again, a Kruskal-Wallis test is performed instead. As for this dataset the assumption of equal distribution between datasets is also violated (see Figure 16), but each group has a relatively large sample size (87-195), this assumption is again ignored but kept in mind for later interpretation.

Also, for this dataset, the Kruskal-Wallis test showed significant differences between the groups (Chi-squared = 126,91, df = 65, *p*-value = 6,908e-06). A pairwise Wilcoxon rank sum test with a Benjamini & Hochberg (1995) adjusted *p*-value shows that groups between which there is no significant difference (thus p > 0,05) are 0,1m-6,5m, 0,1m-6,9m, 0,5m-6,5m, 1,0m-1,5m, 1,0m-6,0m, 1,5m-2,0m, 1,5m-5,0m, 1,5m-5,5m, 1,5m-6,0m, 2,0m-4,5m, 2,0m-5,0m, 2,0m-5,5m, 2,0m-6,0m, 3,0m-3,5m, 3,0m-4,5m, 3,5m-4,0m, 4,5m-5,0m, 4,5m-5,5m, 5,0m-5,5m, 5,0m-6,0m, 5,5m-6,0m, 6,5m-6,9m. Visual analysis shows that these results allow for a grouping into zones, when arrows that point to the same cells are clustered together (Figure 18).

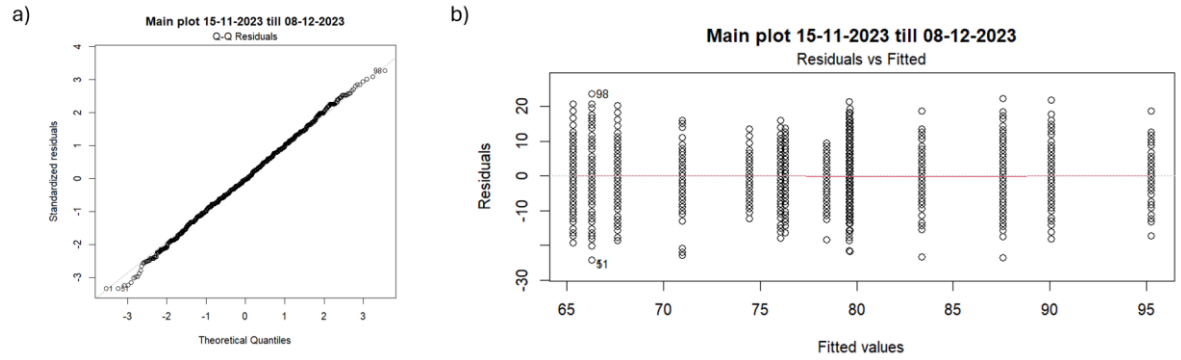

Figure 17.
a) QQ plot of the regression residuals from the Main plot dielectric conductivity measurements dataset of 15-11-2023 till 08-12-2023.
b) Regression residuals plotted against the fitted values for the Main plot dielectric conductivity measurements dataset of 15-11-2023 till 08-12-2023.

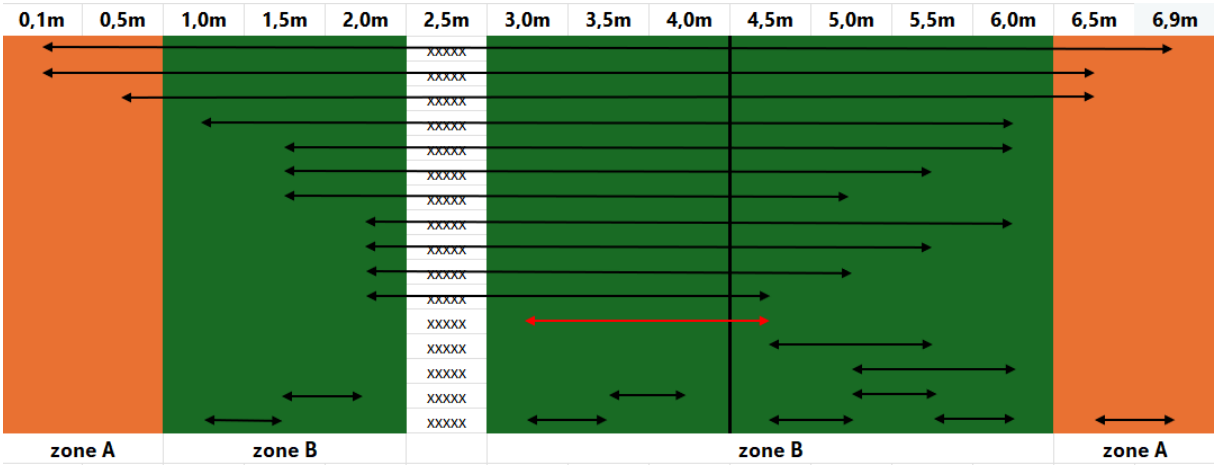

Figure 18. *Visual analysis of the Wilcoxon rank sum test results on the Main plot dielectric conductivity dataset of 15-11-2023 till 08-12-2023. Arrows show between which groups of values there is no significant difference (thus p > 0,05). Coloured planes visualise a suggested grouping into zones.* xxxxx *indicates zone where no measurements have been taken. Red arrow hinders splitting zone B along the tire track (between 4,0m and 4,5m, black line) as was possible in Figure 14.*

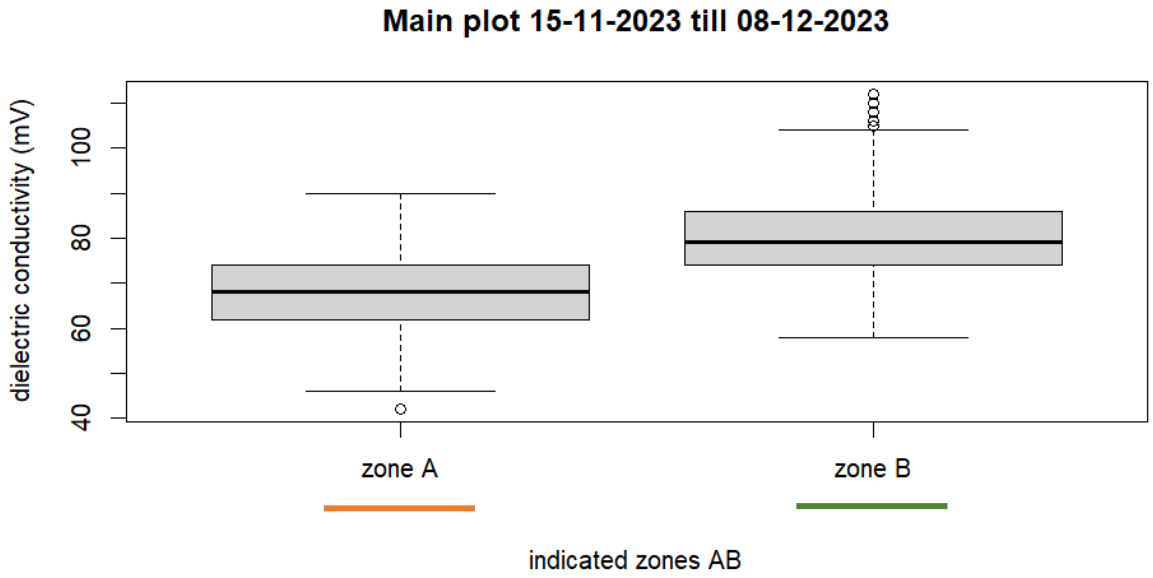

Figure 19.
a) Dielectric conductivity readings in the Main plot during the period 15-11-2023 till 08-12-2023 along each of the five primary transects. Grouping according to zones defined in Figure 18. Data from locations 4,0m and 4,5m were excluded.
(see next page for Figure 19.b)

Statistical analysis was performed comparing the data grouped in two groups (Figure 19.a) as indicated in Figure 18. Data from locations 4,0m and 4,5m were excluded. The Shapiro-Wilk test for normality (W = 0,97751, *p*-value < 2,2e-16) and Levene's test for homoscedasticity (F(2,2323)=7,68, *p*-value = 5,61e-3), indicated non-normality and heteroscedasticity. Consequently a pairwise Wilcoxon rank-sum test has been performed. The test results showed that each group differed significantly.

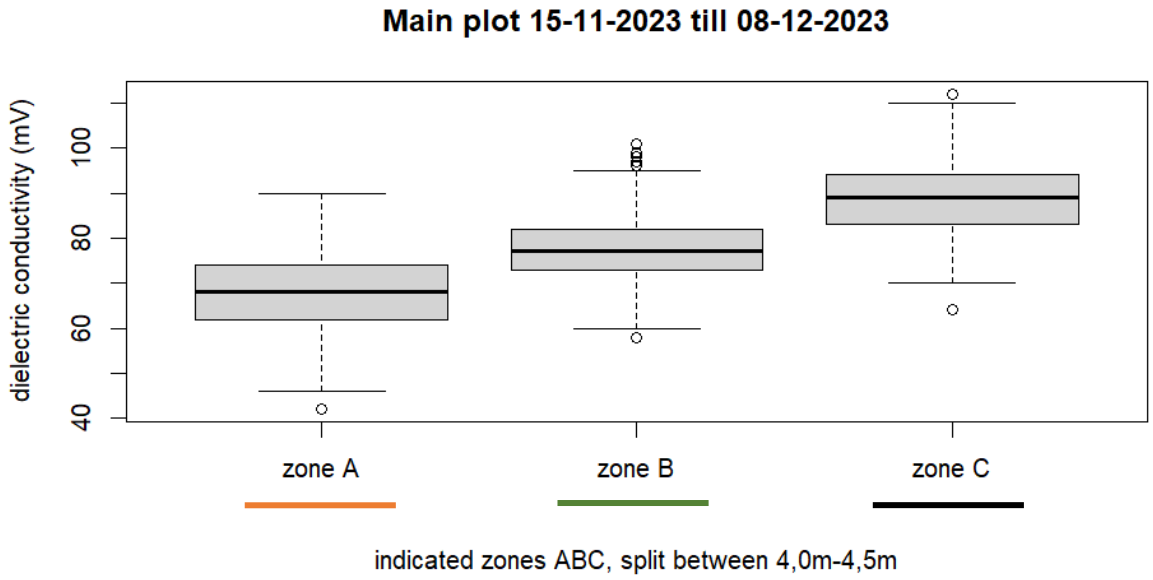

Figure 19.
b) Dielectric conductivity readings in the Main plot during the period 15-11-2023 till 08-12-2023 along each of the five primary transects. Grouping according to zones defined in Figure 18, including the extra split into zone C indicated by the black line in Figure 18. Data from locations 4,0m and 4,5m were excluded.

Similar statistical analysis was performed comparing the data grouped in three groups (Figure 19.b) as indicated in Figure 18, including the split between 4,0m-4,5m indicated by the black line in Figure 18. Data from locations 4,0m and 4,5m were excluded. The Shapiro-Wilk test for normality (W = 0,97751, *p*-value < 2,2e-16) and Levene's test for homoscedasticity (F(2,2322)=13,5, *p*-value = 1,45e-6), indicated non-normality and heteroscedasticity. Consequently a pairwise Wilcoxon rank-sum test has been performed. The test results showed that each group differed significantly.

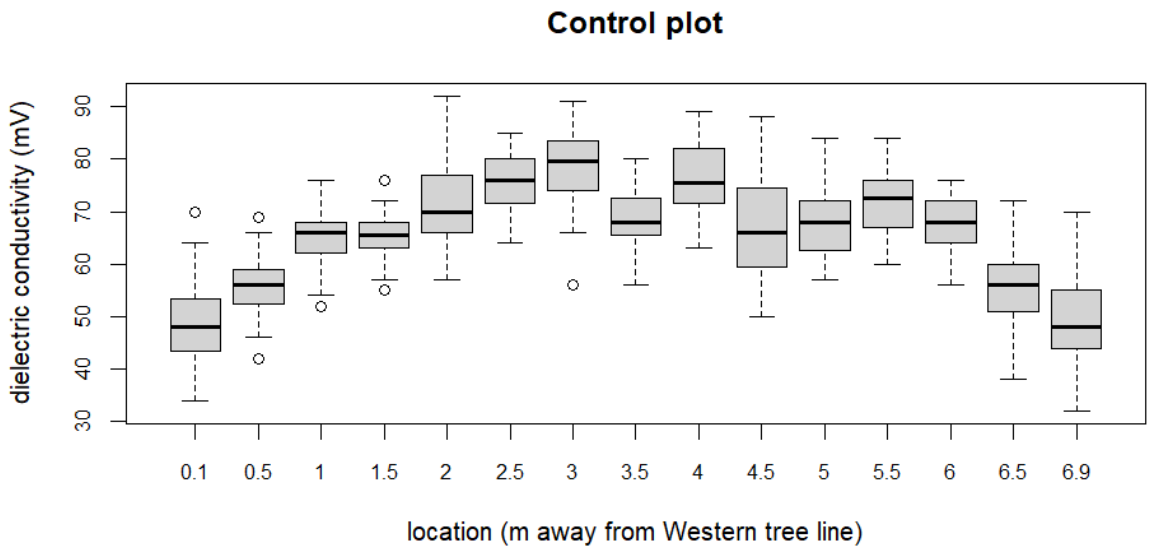

Figure 20. *Dielectric conductivity readings in the Control plot along each of the five primary transects.*

Shapiro-Wilk test results show no indication of non-normality (W = 0,99765, *p*-value = 0,4175), also Figure 21.a shows a normal distribution. However, Levene's test for homoscedasticity shows no equal variance of residuals between the groups (F(14,697)=4,16, *p*-value < 0,001), as does Figure 21.b. Again, under similar argumentation as for the Main plot 15-11-2023 till 08-12-2023 dataset a Kruskal-Wallis test has been performed. This test showed significant differences between groups (Chi-squared = 77,626, df = 58, *p*-value = 0,04363).

To visualise this result, a Wilcoxon rank sum test with a Benjamini & Hochberg (1995) adjusted *p*-value has been performed. It shows that groups between which there is no significant difference (thus p > 0,05) are 0,1m-0,5m, 0,1m-6,5m, 0,1m-6,9m, 0,5m-6,5m, 0,5m-6,9m, 1,0m-1,5m, 1,0m-2,0m, 1,0m-3,5m, 1,0m-4,5m, 1,0m-5,0m, 1,0m-5,5m, 1,0m-6,0m, 1,0m-6,5m, 1,5m-2,0m, 1,5m,3,5m, 1,5m-4,5m, 1,5m-5,0m, 1,5m-5,5m, 1,5m-6,0m, 2,0m-2,5m, 2,0m,3,0m, 2,0m-3,5m, 2,0m-4,0m, 2,0m-4,5m, 2,0m-5,0m, 2,0m-5,5m, 2,0m-6,0m, 2,5m-3,0m, 2,5m-3,5m, 2,5m-4,0m, 2,5m-4,5m, 2,5m-5,0m, 2,5m-5,5m, 2,5m-6,0m, 3,0m-4,0m, 3,0m-4,5m, 3,0m-5,5m, 3,5m-4,0m, 3,5m-4,5m, 3,5m-5,0m, 3,5m-5,5m, 3,5m-6,0m, 4,0m-4,5m, 4,0m-5,0m, 4,0m-5,5m, 4,0m-6,0m, 4,0m-6,5m, 4,5m-5,0m, 4,5m-5,5m, 4,5m-6,0m, 4,5m-6,5m, 4,5m-6,9m, 5,0m-5,5m, 5,0m-6,0m, 5,5m-6,0m, 6,5m-6,9m. This is in agreement with Figure 20. Visual analysis shows that these results allow for a grouping into one general zone, when arrows that point to the same cells are clustered together (Figure 22).

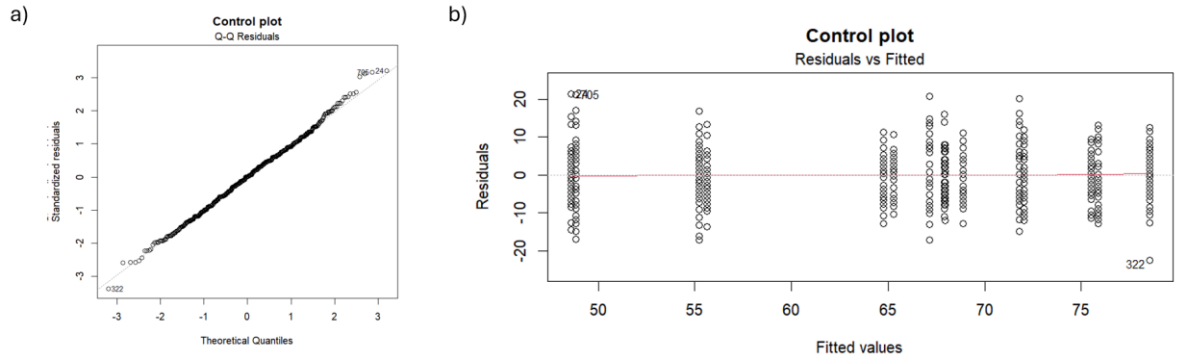

Figure 21.
a) QQ plot of the regression residuals from the Control plot dielectric conductivity measurements dataset.
b) Regression residuals plotted against the fitted values for the Control plot dielectric conductivity measurements dataset.

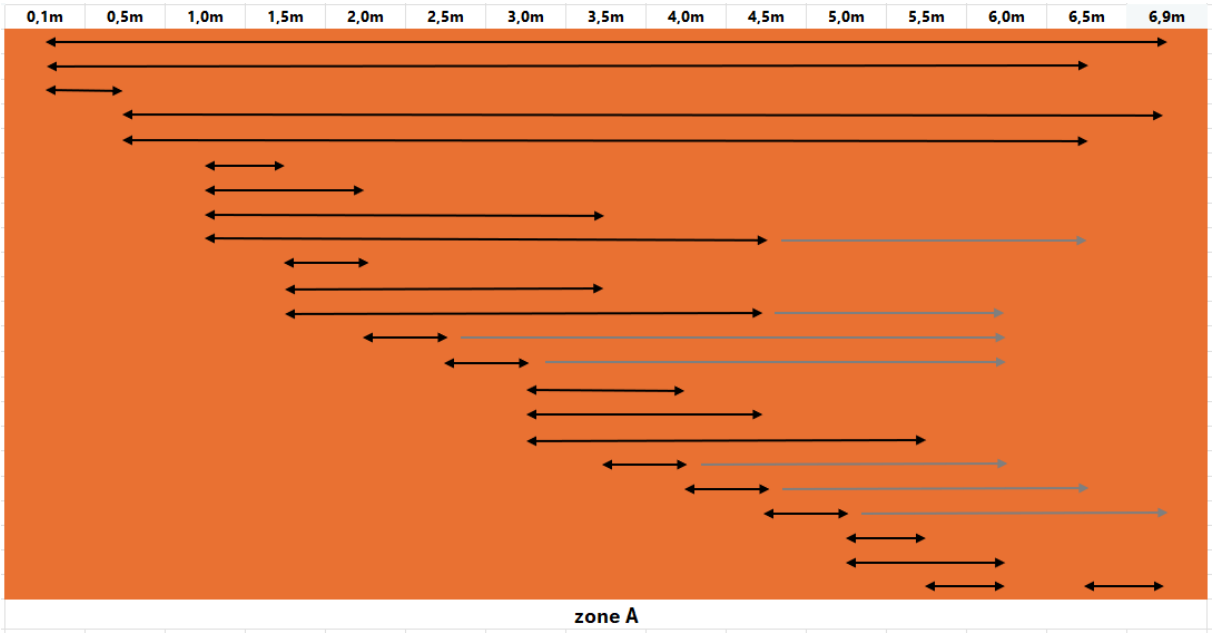

Figure 22. *Visual analysis of the Wilcoxon rank sum test results on the dielectric conductivity dataset of the Control plot. Arrows show between which groups of values there is no significant difference (thus p > 0,05). Grey arrows cover all the neighbouring locations the adjacent black arrow should also point to. Coloured plane visualises a suggested grouping into zones, crossing zone borders of Figure 14.b.*

Statistical analysis: Difference in variance between measuring days

Grouping all measurements from each measuring day together (Figure 23) allows statistical analysis of variance between these groups. For proper analysing of the data all values of date 27-11-2023 and all values of transect 5 of date 16-12-2023 have been removed. A pairwise variance test with a Bonferroni correction (controlling for false positives, allowing missing true positives) shows a significant difference between the variance of the Main plot 01-10-2023 till 26-10-2023 groups relative all Main plot 15-11-2023 till 08-12-2023 groups except 20231026 (26-10-2023) against 20231115 (15-11-2023) and all Control plot groups. For the Main plot 15-11-2023 till 08-12-2023 groups 20231115 (15-11-2023) differs significantly from all the Control plot groups, and 20231204 (04-12-2023) from the first two Control plot groups.

Within the Main plot 01-10-2023 till 26-10-2023 groups 20231001 (01-10-2023) differs significantly from most other groups. 20231013 (13-10-2023), 20231025 (25-10-2023), 20231026 (26-10-2023) all also differ significantly from some other groups. Within the Main plot 15-11-2023 till 08-12-2023 groups, date 20231115 (15-11-2023) differs with all the other groups starting from 20231126 (26-11-2023) onwards. Groups 20231115 (15-11-2023) till 20231123 (23-11-2023) all significantly differ from group 20231204 (04-12-2023). There is no statistical difference in variance between the groups from the Control plot.

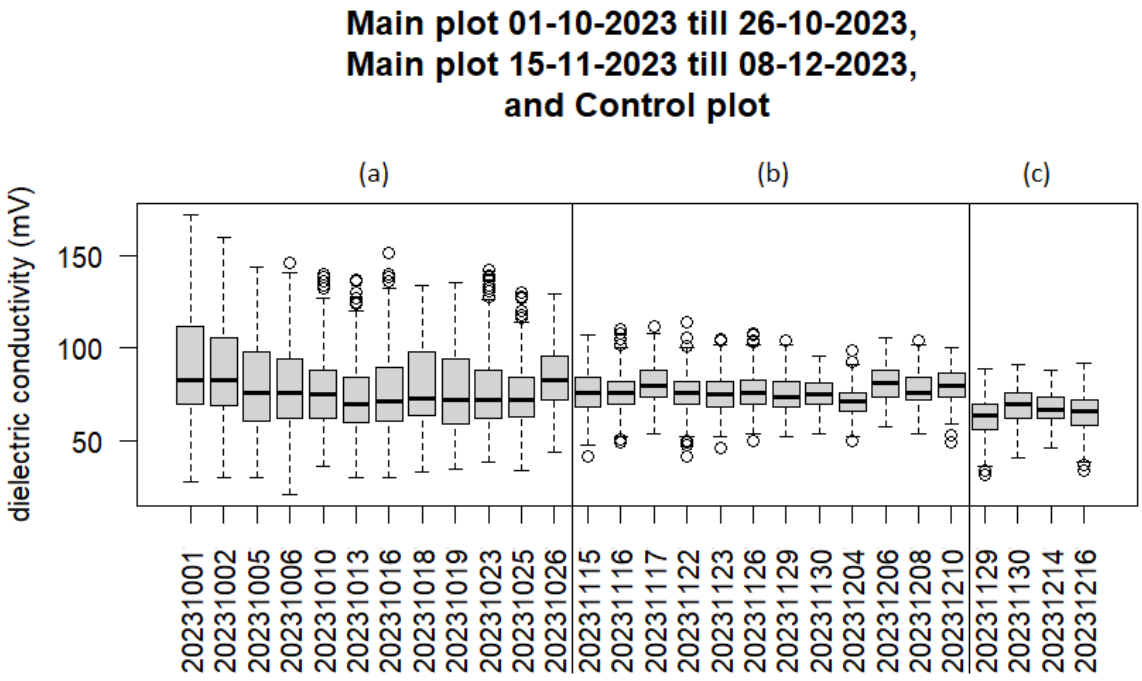

Figure 23. *Boxplot showing grouping of all measurement data per measuring day for (a) Main plot 01-10-2023 till 26-10-2023, (b) Main plot 15-11-2023 till 08-12-2023, (c) Control plot. Date notation YYYYMMDD.*

Figure 24. *Visual analysis of the pairwise variance test (Bonferroni correction) results on grouping of all measurement data per measuring day for (a) Main plot 01-10-2023 till 26-10-2023, (b) Main plot 15-11-2023 till 08-12-2023, (c) Control plot. Arrows show between which groups of values there is a significant difference (thus p < 0,05). Grey arrows cover all the neighbouring locations the adjacent black arrow should also point to. Date notation YYYYMMDD.*

Soil compaction testing

Characteristics analysis

Plotting the average penetration resistance depths for each measurement point along the five (secondary) transects of the Main plot and the five of the Shadow plot shows several noticeable characteristics (Figures 25 and 26). Both the graph of the Main plot averages and the Shadow plot averages show points (2,5m and 4,0m) with a much lower average penetration resistance depth for all three degrees of resistance (200 psi (Shadow plot), 300 psi (Shadow plot), impenetrable (both)) compared to all other measurement points. For the other points the average depth at with impenetrability occurs fluctuates roughly between 9 and 17 cm deep. The average depths at which 200 psi and 300 psi resistance starts in the Shadow plot is less deep for the points 3,0m and 3,5m compared to the points 0,1m-1,5m and 5,0m-6,4m. When removing the upper layer of uncompacted soil in the Main Plot a more compacted layer of soil appears with trenches and hills (Figure 27).

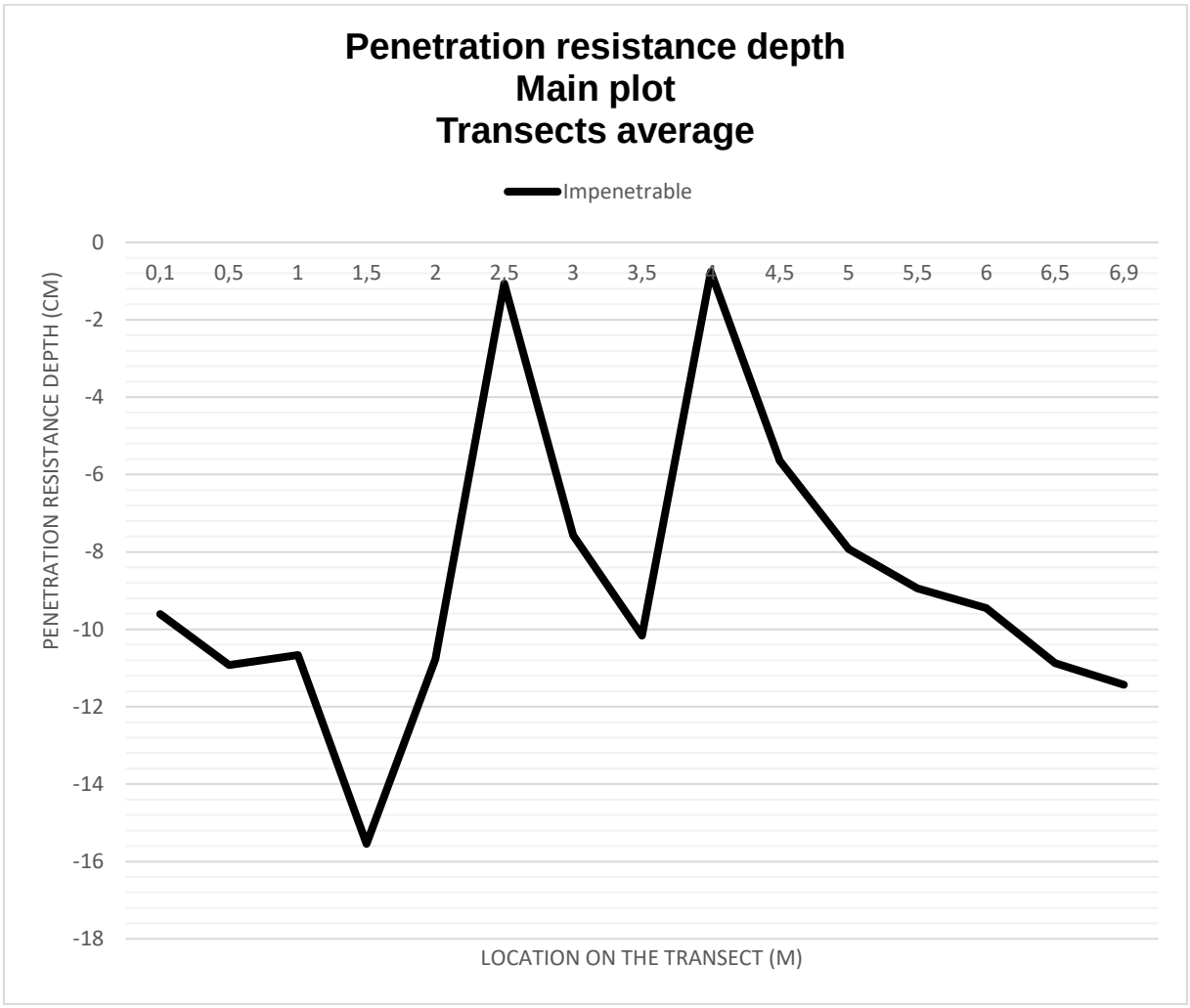

Figure 25. *Penetration resistance depth in the Main plot, average of all five measured transects.*

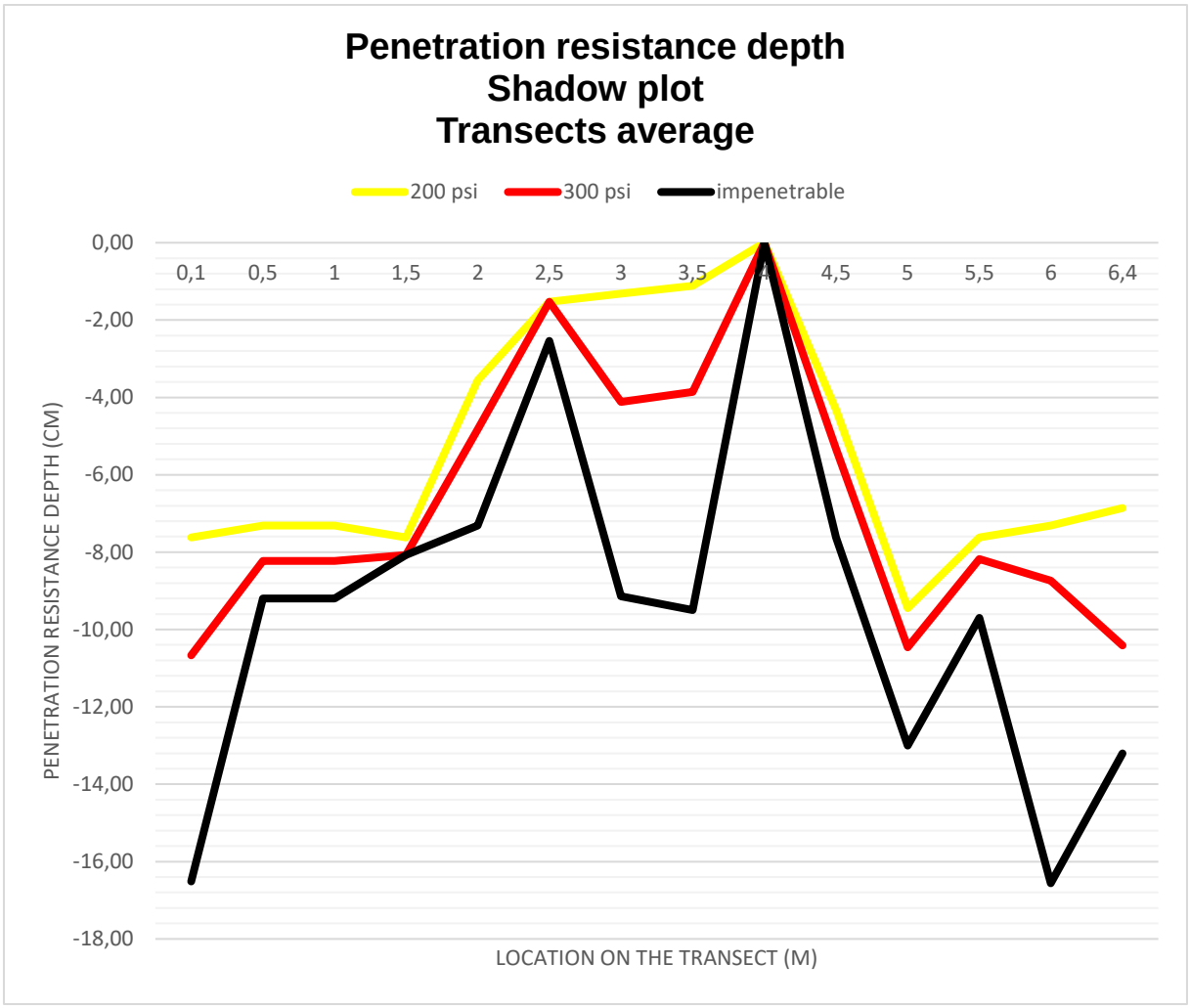

Figure 26. *Penetration resistance depth in the Shadow plot, average of all five measured transects.*

Figure 27. *Uncovered compacted soil layer in Main plot.*

Statistical analysis

Further statistical analysis has been performed to show if there are any significant differences between the locations concerning penetration resistance depth.

MAIN PLOT - IMPENETRABLE RESISTANCE

In the Main plot, along each of the five primary transects, the depths at which the soil became impenetrable has been measured. For each distance away from the Western tree line ("location") the measurements of all transects have been grouped together. These groups are statistically analysed.

Shapiro-Wilk normality test (W = 0,97084, *p*-value = 0,08079) shows no indication of non-normality, also the QQ residuals plot indicates normality (Figure 28.a). Levene's test F(14,60)=0,872, *p*-value = 0,591, shows equal variance of residuals between groups, just as Figure 28.b. Therefore, the assumptions of one-way ANOVA are met. A one-way ANOVA test gives *F*(14,60)=5,267, *p*-value = 2,33e-06, indicating significant differences between the groups. The Tukey HSD test shows that the following groups differ significantly (p < 0,05): 0,1m-2,5m, 0,1m-4,0m, 0,5m-2,5m, 0,5m-4,0m, 1,0m-2,5m, 1,0m-4,0m, 1,5m-2,5m, 1,5m-4,0m, 1,5m-4,5m, 2,0m-2,5m, 2,0m-4,0m, 2,5m-3,5m, 2,5m-6,5m, 2,5m-6,9m, 3,5m-4,0m, 4,0m-6,0m, 4,0m-6,5m, 4,0m-6,9m. These groups are visually depicted in Figure 29.

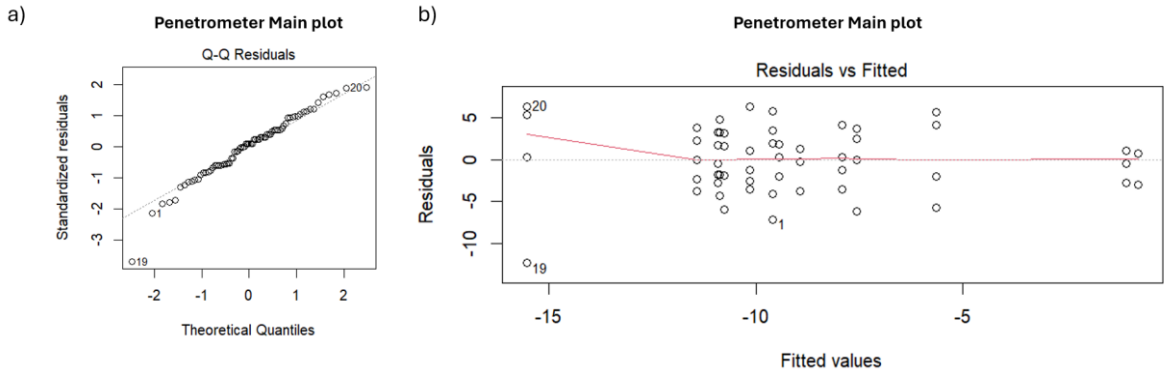

Figure 28.

a) QQ plot of the regression residuals from the Main plot penetrometer impenetrable depth dataset.

b) Regression residuals plotted against the fitted values for the Main plot penetrometer impenetrable depth dataset.

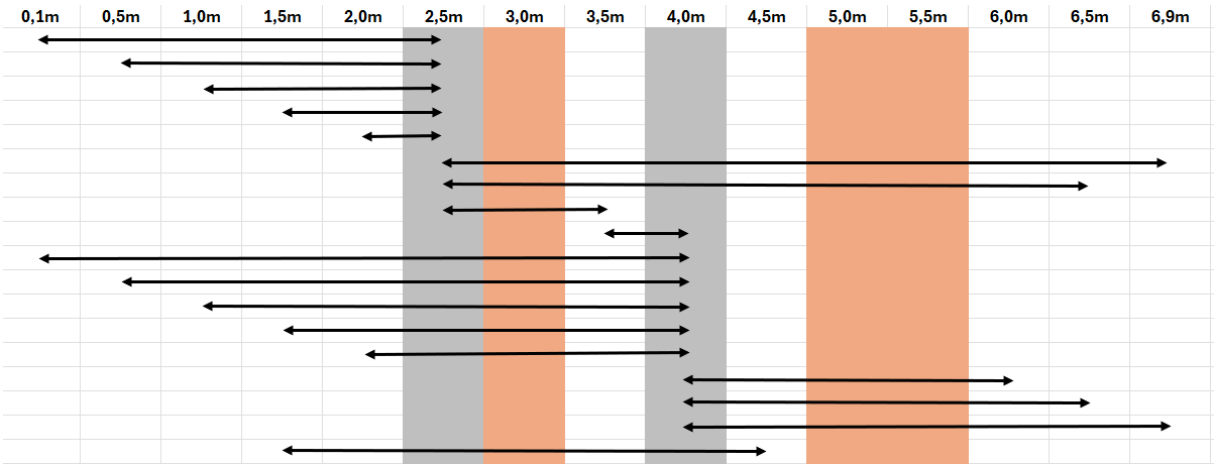

Figure 29. *Visual analysis Tukey HSD results from the penetrometer Main plot impenetrable depth dataset. Arrows show groups that significantly differ (p-value < 0,05). Grey indicates locations that differ with most other groups. Red indicates locations that differ with no other group.*

SHADOW PLOT - 200 PSI RESISTANCE

Similar analysis have been performed for the penetrometer measurements in the Shadow plot, where not only the depth of impenetrability, but also 200 psi resistance depth and 300 psi resistance depth has been measured. Grouping was done in similar manner as for the Main plot impenetrability depth dataset.

Shapiro-Wilk test results (W = 0,91028, *p*-value = 0,0001012), as also Figure 30.a indicate non-normality. Levene's test results $F(13,56) = 0,854$, *p*-value = 0,603, as also Figure 30.b show equal variance of residuals between groups. The assumptions for a Kruskal-Wallis test are therefore met, which shows no significant differences between the groups (Chi-squared = 6,3163, df = 10, *p*-value = 0,788). However, the boxplot (Figure 33.a) indicates visual differences between several groups, mainly locations 2,5m and 4,0m, and 2,0m and 4,5m relative to the other locations.

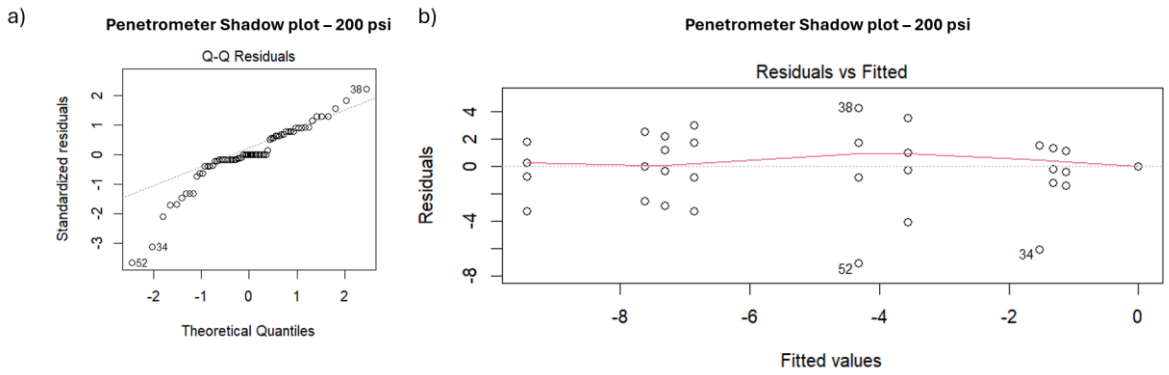

Figure 30.
a) QQ plot of the regression residuals from the Shadow plot penetrometer 200 psi resistance depth dataset.
b) Regression residuals plotted against the fitted values for the Shadow plot penetrometer 200 psi resistance depth dataset.

SHADOW PLOT - 300 PSI RESISTANCE

Shapiro-Wilk test results (W = 0,8913, *p*-value = 1,788e-05), as also Figure 31.a indicate non-normality. Levene's test results $F(13,56) = 0,827$, *p*-value = 0,631, as also Figure 31.b show equal variance of residuals between groups. The assumptions for a Kruskal-Wallis test are therefore met, which shows no significant differences between the groups (Chi-squared = 9,8017, df = 12, *p*-value = 0,6334). However, the boxplots (Figure 33.b) indicate visual differences between several groups, mainly locations 2,5m and 4,0m, and 2,0m and 4,5m relative to the other locations.

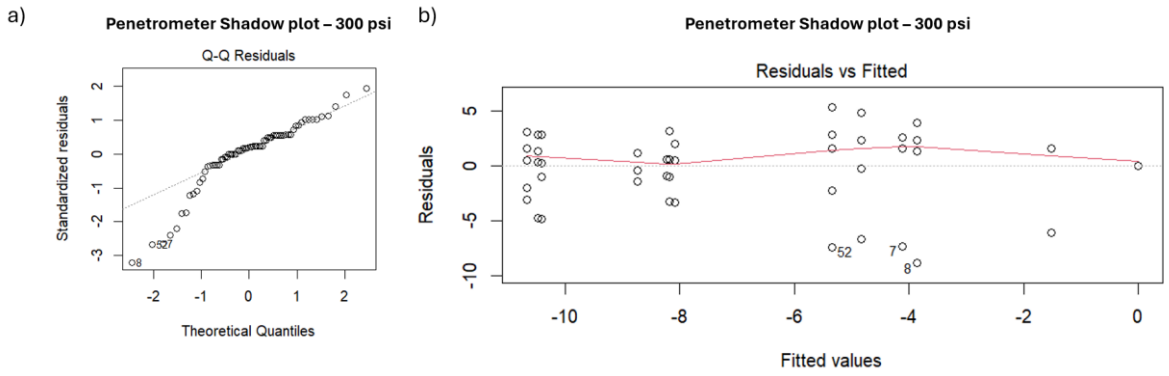

Figure 31.

a) QQ plot of the regression residuals from the Shadow plot penetrometer 300 psi resistance depth dataset.

b) Regression residuals plotted against the fitted values for the Shadow plot penetrometer 300 psi resistance depth dataset.

SHADOW PLOT - IMPENETRABLE RESISTANCE

Shapiro-Wilk test results (W = 0,93745, *p*-value = 0,001687), as also Figure 32.a indicate non-normality. Levene's test results ($F(13,56) = 0,983$, *p*-value = 0,480), as also Figure 32.b show equal variance of residuals between groups. The assumptions for a Kruskal-Wallis test are therefore met, which shows no significant differences between the groups (Chi-squared = 9,8017, df = 12, *p*-value = 0,6334). However, the boxplot (Figure 33.c) indicates visual differences between several groups, mainly locations 2,5m and 4,0m relative to the other locations.

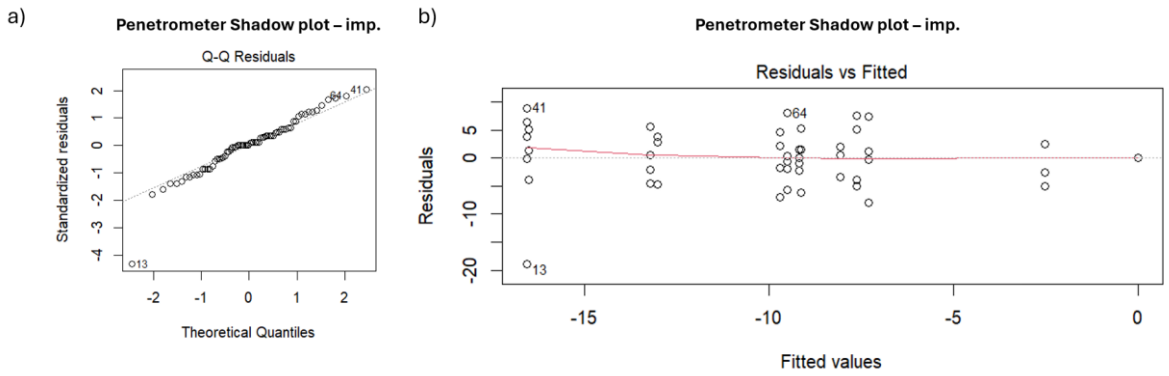

Figure 32.
a) QQ plot of the regression residuals from the Shadow plot penetrometer impenetrable depth dataset.
b) Regression residuals plotted against the fitted values for the Shadow plot penetrometer impenetrable depth dataset.

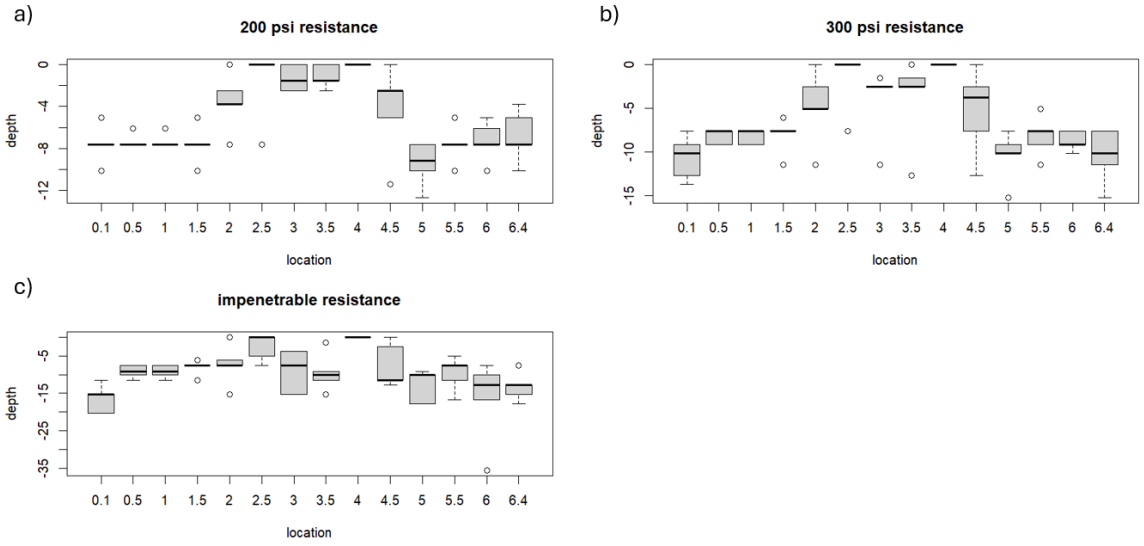

Figure 33. *Boxplots of the Shadow plot a) 200 psi, b) 300 psi, and c) impenetrable resistance depth measurements.*

Ground cover analysis

Obtained ground cover percentages after point intercept analysis (Table 1).

Label	Description	Main plot Till area	Main plot No-till area	Shadow plot Till area	Shadow plot No-till area
Tumbleweed	Tumbleweed	0,0 %	3,3 %	0,0 %	3,5 %
Plant	Living plant, other than tumbleweed	0,0 %	0,0 %	0,0 %	2,4 %
Litter	Organic litter	4,2 %	7,7 %	3,4 %	20,9 %
Soil	Bare soil or stone	95,7 %	88,3 %	92,9 %	72,0 %
Unknown	Uncharacterised pixel	0,1 %	0,7 %	3,7 %	1,3 %

Table 1. *Average percentage ground cover type per analysed area.*

Tool validation

The relationship between %Δsample weight and soil dielectric conductivity is assumed to be linear, as it are two different methods to approach volumetric water content of the soil. The data is not obtained through random sampling, but purposefully obtained at specific locations along the transect. However, since the independent and dependent variable in theory should be linear, non-random sampling helps to answer the research question and is therefore appropriate.

Sieving the soil samples made clear that stones had been present in the measuring zones during dielectric conductivity measurements taking, which could have influenced measured values. No later than after 3 rounds of heating each soil sample reached temperatures above 100 °C. In Table 2 the average dielectric conductivity values and Δsample weight per location along primary transects 1 and 2 of the Shadow plot are shown.

	Transect 1	**Transect 1**	**Transect 2**	**Transect 2**
Location (m)	**Dielectric conductivity (mV)**	**%Δsample weight (g)**	**Dielectric conductivity (mV)**	**%Δsample weight (g)**
0,1	45	2,64	44 1/3	0,91
1,5	62 2/3	3,22	56	2,81
2,5	99 1/3	3,49	106	1,59
3	103	3,50	82 2/3	1,58
3,5	79	3,29	88 1/3	1,47
4,25	133	3,26	104	1,61
5	71 2/3	3,12	66	1,50
6,4	38 1/3	2,82	36	0,96

Table 2. *Average dielectric conductivity values and %Δsample weight per location along primary transects 1 and 2 of Shadow plot.*

The linear regression analysis for values obtained for Shadow plot transects 1 and 2 with %Δsample weight as the independent variable and dielectric conductivity as the dependent variable is not significant, $F(1.14)=1{,}168$, $p > 0{,}05$ (Figure 34). The linear regression analysis for values obtained for solely Shadow plot transect 1 with %Δsample weight as the independent variable and dielectric conductivity as the dependent variable is significant, $F(1.6)= 8{,}159$, $p < 0{,}05$ (Figure 35), for solely transect 2 values it is not significant, $F(1.6)= 0{,}2441$, $p > 0{,}05$. A Cook's Distance test on the transect 1 value points shows that the value point with the largest influence on the location of the regression line is (3,26;133), with $D = 0{,}408\ldots$ (Figure 36).

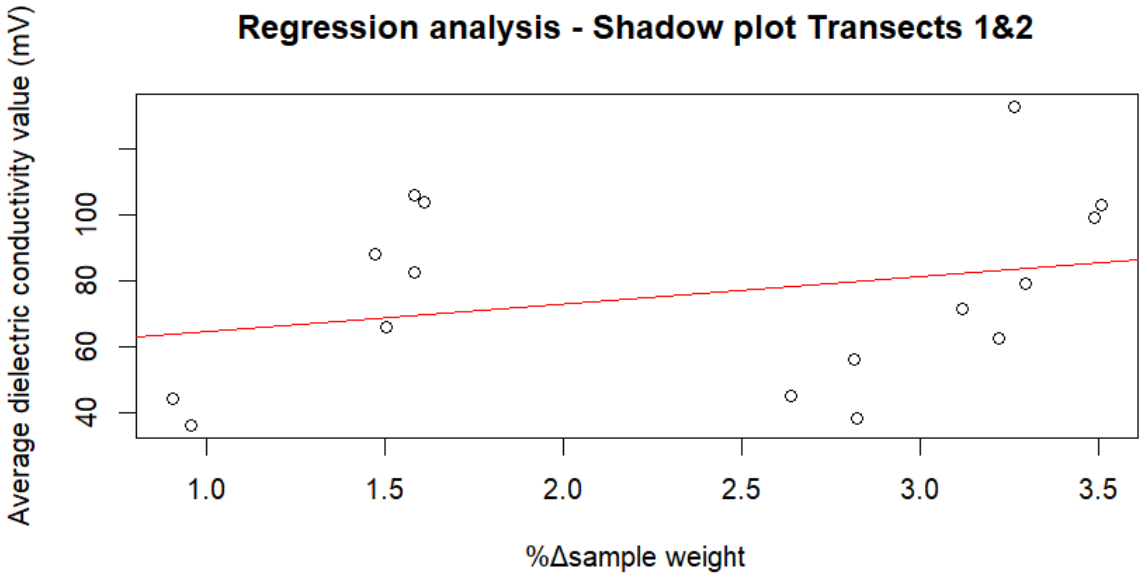

Figure 34. *Regression analysis on obtained dielectric conductivity and %Δsample weight values Shadow plot primary transects 1&2.*

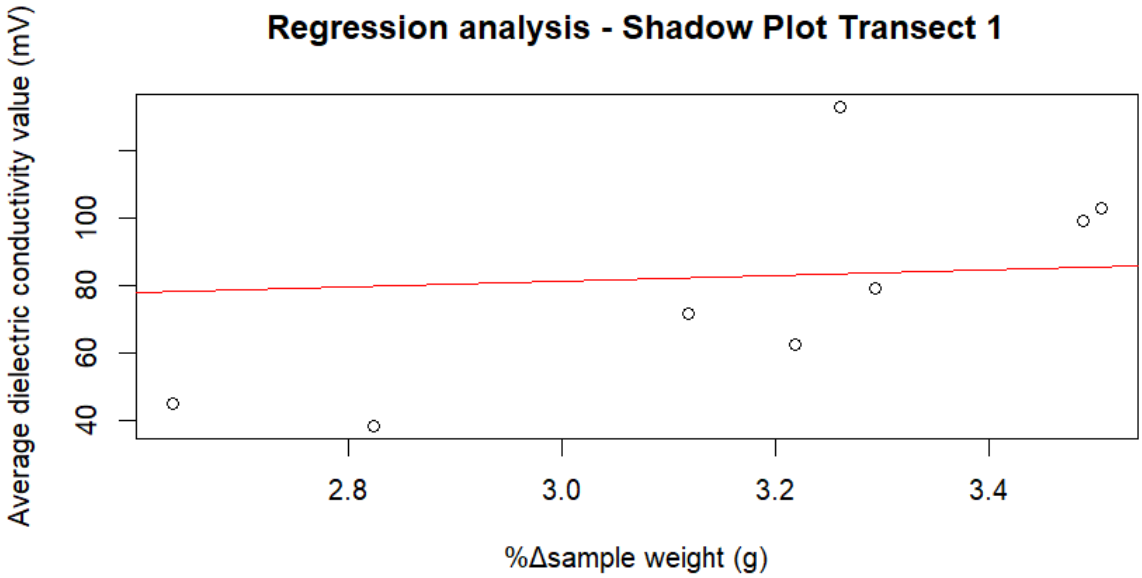

Figure 35. *Regression analysis on obtained dielectric conductivity and %Δsample weight values Shadow plot primary transect 1.*

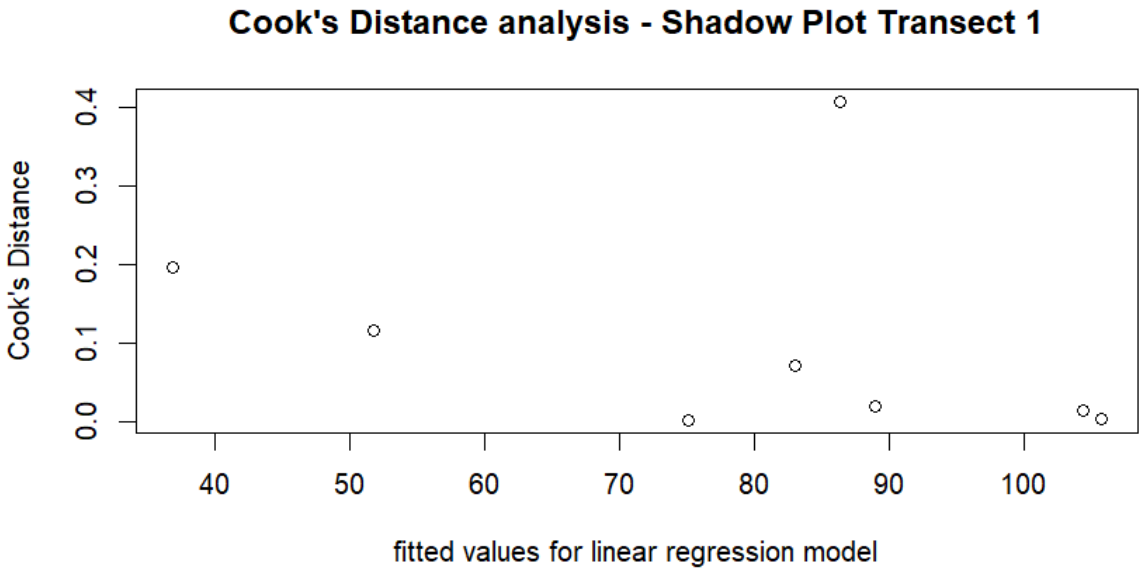

Figure 36. *Results of Cook's Distance test on the value points and accompanying regression line of Transect 1.*

Sensor bias testing

The differences have been calculated between the sensor readout of when the sensor was held by a hand and when not. Table 3 shows for each set of measurements the minimal difference and the maximal difference that showed up in the dataset. The measured values in mV have therefore first been converted to % soil moisture ($\theta_{\%}$). Delta-T Devices Ltd (2016, p. 29) shows that a reading of 45 mV or lower gives a soil moisture value < 0, this still allows for the calculation of a difference between the two measuring methods. The analysis showed an absolute increase in derived $\theta_{\%}$ values between 0,13973 and 2,262954 when the sensor was held, which corresponds to a 2,083333 % to 35 % increase in readout Dielectric conductivity values. For the deviation of the calculated % soil moisture when sensor head is held the data has a Median of 0.9621567, a Q1 of 0.7747683 and a Q3 of 1.1044537 (Figure 37).

Physical quantity / Measurement set	Δ Dielectric conductivity (mV)		Δ % Dielectric conductivity (mV)		Δ % soil moisture (%vol)	
	min	**max**	**min**	**max**	**min**	**max**
20231206 (Main plot)	4	19	4,545455	26,78571	0,471533	2,262954
20231208 (Main plot)	3	16	4,054054	25,92593	0,374905	2,028695
20231210 (Main plot)	3	16	3,947368	22,85714	0,371872	1,979749
20231214 (Control plot)	1	16	2,083333	35	0,13973	2,149214
20231216 (Control plot)	2	16	4,109589	29,41176	0,298373	1,625213
Most extreme value	1	19	2,083333	35	0,13973	2,262954

Table 3. *The maximum and minimum difference in dielectric conductivity readout, maximum and minimum in relative difference in dielectric conductivity readout, and maximum and minimum in relative difference in calculated soil moisture in each measurement set between a hand holding and not holding the sensor. Positive values denote that when a handheld the sensor, the read-out value was higher compared to when the sensor was not held.*

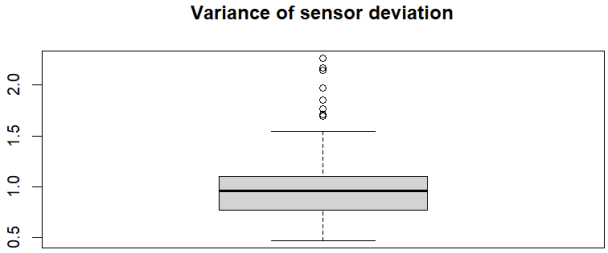

Figure 37. *Boxplot showing spread of calculated % soil moisture deviation when sensor head is held with hand. Boxplot includes the data of all datasets mentioned in Table 3.*

Conclusion

This research tried to answer two research questions. The research questions were 1) *What is the spatial pattern of topsoil moisture content in a Mediterranean rainfed strip-tilled Almond orchard, Southeast Spain?*, 2) *What is the temporal pattern of topsoil moisture content in a Mediterranean rainfed strip-tilled Almond orchard, Southeast Spain?* To answer these research questions in situ quantitative research has been done on dielectric conductivity and other soil characteristics. The research knew several separate research lines.

The obtained results showed that dielectric conductivity values increase away from the almond trees (Figures 6 and 12), peaking however in the area that seems to have the highest compaction in the topsoil (upper 5,1 cm) (Figures 6, 14, 25, and 26). These areas of highest compaction are not proven to differ significantly (Figure 33), however are deduced from visual analysis on Tukey HSD test results (Figure 29). The dielectric conductivity values thus did not peak farthest away from each almond tree, in the middle of a transect between two almond trees. The values in the Control plot did also not peak farthest away from the trees (Figures 8 and 20). However, the dielectric conductivity values differed significantly between different zones in both the Main plot datasets (Figures 14, 15, 18, and 19), but not in the Control plot dataset (Figure 22). The two Main plot datasets do not split in the same zones (Figures 14 and 18). Lowest and highest derived topsoil moisture content values from the Main plot dielectric conductivity measurements dataset 01-10-2023 till 26-10-2023 were -2,6 and 14,0 %vol, which is below an estimated permanent wilting point of 17,5 %vol (Supplement B).

Dielectric conductivity value patterns thus turn out to partly relate to soil compaction levels. In the research field it is generally accepted that topsoil moisture content strongly correlates to soil dielectric conductivity values. A performed tool validation test left it inconclusive whether in higher compacted areas the moisture content was indeed higher, or whether a higher compaction resulted in a higher sensor dielectric conductivity readout without an actual rise in moisture content (Figure 36).

Regarding change over time, there is no clear pattern visible in dielectric conductivity standard deviation values for each observation location in each of the five primary transects of the Main plot dataset 01-10-2023 till 26-10-2023 and Control plot (Figures 9 and 11). However, highest SD values within each transect are seen at 0,1m and 6,9m, and in the 2,0m-4,5m zone. The 0,1m and 6,9m location measurements are the groups with the lowest average dielectric conductivity values (Figures 6, 12, and 14.b), the 2,0m-4,5m zone is where higher soil compaction is present (Figure 25 and 29). Therefore, indicating a relationship between SD and either topsoil moisture content and/or soil compaction influencing sensor readout. However, the total measurements per day have a larger spread in the Main plot 01-10-2023 till 26-10-2023 dataset relative to the Main plot 15-11-2023 till 08-12-2023 dataset and Control

plot dataset (Figure 24), indicating a smaller difference between measured values at the different locations within the last two datasets relative to the first one.

Thus, the answer to the first research question is that in the strip tilled Main plot the measured dielectric conductivity values increased away from the almond trees, peaking not in the middle between two almond trees, but in the areas with highest topsoil compaction, always staying below permanent wilting point threshold. Dielectric conductivity measurements differ significantly in the no-till strip relative to the tilled areas (Figures 14, 15, 18, 19, 22, and 23). The answer to the second research question is that the highest variance in measured dielectric conductivity values is seen at 0,1m and 6,9m and in the 2,0m-4,5m zone for both the strip tilled Main plot and full tilled Control plot, with highest measured values spread per day in the Main plot 01-10-2023 till 26-10-2023 dataset relative to the Main plot 15-11-2023 till 08-12-2023 dataset and Control plot dataset. For both research questions it is still unsure whether these measured values directly correlate with topsoil moisture content, or whether they are partly influenced by topsoil compaction levels. In case of direct correlation, derived topsoil moisture content values are off by 0,14-2,26 %vol (median ~1,0%), due to the sensor being influenceable through touch (Table 3, Figure 37).

Discussion

This research started with the hypothesises that 1) *Topsoil moisture content increases away from the almond trees, and, independent from position relative to an Almond tree, is higher in the no-till areas compared to the till areas*, and 2) *There is more temporal difference in topsoil moisture content in the tilled zone compared to the no-till zone*. The results show that indeed dielectric conductivity values, indicating topsoil moisture content, increase away from the almond trees and that it is significantly higher in the no-till areas compared to the till areas. However, the Standard Deviation of dielectric conductivity values, indicating temporal change, is highest (see Figure 11) at locations in zones A and C defined in Figure 14, which do not refer to the specific till (zone B) and no-till (zone D) zones of the plot. No statistical test could be performed (as done for Figure 15) due to too low *n* values based on Figure 11. It is yet unclear however, whether soil compaction affects sensor readout and thus results.

The results should be interpreted with a critical attitude towards the Control measurements. The Control plot has too small group sizes (effects 0,5, *p*-value 0,05, power 0,8, requires group size = min. 64), making Type II errors more likely. Also, Figure 8 hints at the interpretation that for proper Control group analysis the Control plot needed to be in (renewed) full till condition longer than it had been. As it could be that the measured dielectric conductivity which Figure 8 shows to peak at locations 2,0m, 2,5m, or 3,0m in the different transects indicate a former compaction zone, like in Figure 25, however, slightly spread out due to tilling practices. This is supported by the consistent peak at location 4,0m in both Figures 6 (Main plot) and 8 (Control plot) for all transects (4,5m for transect 2 Figure 6), Figure 11 indicating relative large change of moisture content over time at locations where the soil seems to be spread out, and Figure 38 showing soil chunks in the control plot 2,0-3,0m zone that indicate compacted soil not being broken up completely (which also hinders proper measuring). These high compaction zones are most likely caused by multiple rides of traffic, driving in almost but not fully straight lines, as seen in Figure 2. This is in accordance with the paper of Biddoccu et al. (2016), which states that TSWC is higher in traffic lanes as here the soil is sealed off as a result of the compaction. It is also possible that the tillage activity in the Control plot close to the measuring period affected the soil moisture content in this plot in general, as the field average dielectric conductivity values in the Control plot seems much lower than the field average values from the two Main plot measuring periods (2,67686 against 4,22425 and 4,09937).

In case the formerly compacted areas of the Control plot were indeed not properly crumbled through tillage and/or needed to be in full till condition longer than they had been to function as a proper control, Figures 9 and 11 hint at two different things; Either that soil compaction is related to higher topsoil moisture content instability or that soil compaction influences sensor readout. This is backed-up by, and allows for, reversed interpretation, that a very compacted but airy area hinders soil readout. This would explain the higher Standard Deviation (SD) at locations 0,1m and 6,9m as found in Figure 9 (transects 4 and 5), Figure 10 (transect 1), and

Figure 11. Figure 39 shows how soil near a tree trunk could be indeed compacted but airy. However, in a non-Mediterranean setting a negative correlation between mean plot soil moisture content and spatial variability has been found (Korres et al., 2015). Thus, stating that spatial variability is to be expected in a plot with low average soil moisture content. With the pore size distribution and thus soil texture type controlling the maximum value of the soil moisture SD (Vereecken et al., 2007).

The use of measuring tape hindered exact determination of locations 4,0m and 4,5m for Main plot dataset 01-10-2023 till 26-10-2023, which probably explains why zone C in Figure 14 differed in size at locations 2,5m and 4,0m-4,5m. For Main plot dataset 15-11-2023 till 08-12-2023 the use of measuring rope allowed more concise location determination. However, the tire track related compaction was not an exact straight line, resulting in data gaps alternating at locations 4,0m and 4,5m in Figures 7 and 10 since here the sensor was not used to avoid compaction related sensor damage. This explains why in Figure 18 a split of zone B was expected between 4,0m and 4,5m similar to Figure 14.

For more concise results, measuring locations should be determined with a measuring rope or transect long measuring tape from the start. The sensor head should not be in contact with any material, only the air. A more sustainable solution should be used to allow continues measurements in highly compacted soil areas, preventing data gaps like in Figures 7 and 10. It should be taken into account that not only precipitation but also the time of the day, air temperature, and air humidity might influence dielectric conductivity readouts, which could explain differences in SD seen in Figure 24. Soil compaction measurements should be improved by describing how the soil's surface is possibly not smooth, giving a better interpretation of the depth of any compaction layer. Again, a larger group size is necessary to prevent Type II errors that possibly occurred while analysing whether there is a significant difference in compaction between several locations (Figure 33). Different quality images need to be used to properly differentiate between different species of ground cover vegetation. The soil texture jar test possibly should be performed without detergent, as is now also instructed in an updated manual (Jeffers, 2023). Temporal analysis of soil moisture after rainfall was not possible in this research due to the lack of sufficient rainfall (Supplement C), which asks for research protocols with rain simulation. To unveil the relationship between soil compaction and sensor readout, the in this report proposed Tool validation methodology could be improved by drying the soil samples in the microwave the same day as the dielectric conductivity measurements are taken in the field and the soil samples are taken from the field to prevent assumed drying out.

The dielectric conductivity readouts indicated soil moisture contents between -2,6 and 14,0 %vol. However, the determined soil texture of the orchard relates to an estimated permanent wilting point of 17,5%. Statistical relationships between soil water content and clay or clay+silt fraction indicate an even lower estimated permanent wilting point (Farrick et al., 2018). The negative %vol value can either be explained, again, by soil airiness, or by insensitivity of the sensor for the actual soil moisture content (Mittelbach et al., 2012; Vereecken et al., 2007). In case of the last, at least a sensor calibration would have been

required as described in Delta-T Devices Ltd. (2016, p.42-48), a procedure for which the equipment was not available during this research. Nonetheless, the sensor is known to have a bias up to a maximum of 3 %vol (Delta-T Devices Ltd., 2016, p.33). The maximum derived soil moisture content value laying below estimated permanent wilting point indicates that the almond trees do not subtract their water from the field's topsoil as it would not support plant growth. This is supported by the found absence of roots in the topsoil (Supplement A), in accordance with the description of Van Wesemael et al. (2006) on how Almond trees in orchards develop deep root systems after the top roots are cut off through tilling.

Though, point intercept analysis did indicate some spontaneous vegetation growing in the no-till areas of the plots (Table 1). Therefore, it should be considered that the estimated permanent wilting point is off, or that the spontaneous vegetation have a higher than common water suction capacity (Kirkham, 2005). The low dielectric conductivity values near the tree trunk lines could not only be explained by degree of compaction, but also by extraction of water from the soil by the Almond trees. An alternative interpretation of the no-till zone having lower moisture content relative to the tire track zones could be the presence of water extracting spontaneous vegetation, being said that the ground coverage was very little (Table 1). The insights in this paragraph bring new perspectives in the research topic on indirect water competition between ground cover vegetation and tree crops.

This research gave insight into the relationship between soil compaction and dielectric conductivity readout values. Bringing awareness to the fact that either degree of compaction wrongly affects readout values, or that higher compacted areas store more moisture. If indeed soil compaction influences dielectric conductivity sensor readouts, it would have mayor implications for past and future research depending on similar sensors. Therefore, the in this report proposed tool validation methodology is of great value to the research field.

Still, the obvious scarcity of water in the field leads to two interesting new research objectives. Shifting the focus on the topsoil being a moisture reservoir to the topsoil being a moisture let-through raises the question of the topsoil's role in replenishing deeper moisture reservoirs. Future research could therefore focus on the effect of no-till strips on water infiltration and hydrological conductivity, and soil evaporation and evapotranspiration with or without vegetation in the no-till strips in almond orchards, as has been done by Zuazo et al. (2009) for olive orchards. Secondly, future research could focus on moisture patterns in deeper soil layers. The aim would be to find out more about deep soil moisture availability and moisture harvesting by almond trees, looking at for example the influence of compaction layers (Figure 27). A possible non-disruptive methodology based on electrical resistivity tomography suitable for this research aim has already been proposed by Acosta et al. (2022). Results would help understand on mesoscale which locations are more suitable for rainfed orchards, differing possibly even within one farm, and how the need for irrigation possibly is root depth and therefore also almond crop age dependent (Ding et al., 2024).

Figure 38. *Part of Control plot 2,0m-3,0m soil zone, indicating compacted soil not being broken up completely after tillage practises.*

Figure 39. *Picture of the soil near an almond tree trunk of the Main plot. The right knot in the measuring rope indicates 0,0m away from the tree trunk, the left knot indicates 6,9m (inverse 0,1m) away from the tree trunk. The present pencil is an artifact.*

References

Acosta, J. A., Gabarrón, M., Martínez-Segura, M. A., Martínez-Martínez, S., Faz, Á., Pérez-Pastor, A., Gómez-López, M. D., & Zornoza, R. (2022). Soil water content prediction using Electrical resistivity tomography (ERT) in Mediterranean tree orchard soils. *Sensors*, *22*(4), 1365. https://doi.org/10.3390/s22041365

Andrade, C., Contente, J., & Santos, J. A. (2021). Climate change projections of dry and wet events in Iberia based on the WASP-Index. *Climate*, *9*(6), 94. https://doi.org/10.3390/cli9060094

Benjamini, Y., and Hochberg, Y. (1995). Controlling the false discovery rate: a practical and powerful approach to multiple testing. *Journal of the Royal Statistical Society Series B*, **57**, 289–300. doi:10.1111/j.2517-6161.1995.tb02031.x.

Biddoccu, M., Ferraris, S., Opsi, F., & Cavallo, E. (2016). Long-term monitoring of soil management effects on runoff and soil erosion in sloping vineyards in Alto Monferrato (North–West Italy). *Soil And Tillage Research*, *155*, 176–189. https://doi.org/10.1016/j.still.2015.07.005

Booth, D. T., Cox, S. E., & Berryman, R. D. (2006). Point Sampling digital imagery with 'SamplePoint.' *Environmental Monitoring and Assessment*, *123*(1–3), 97–108. https://doi.org/10.1007/s10661-005-9164-7

Briggs, L. T., & Shantz, H. L. (1912). The Wilting Coefficient and its Indirect Determination. *Botanical Gazette*, *53*(1), 20–37. https://www.jstor.org/stable/2467365

CAP 2023-27. (2024, March 7). Agriculture and Rural Development. https://agriculture.ec.europa.eu/common-agricultural-policy/cap-overview/cap-2023-27_en

Delta-T Devices Ltd. (2016). *User Manual for the SM150t Soil Moisture Sensor* (SM150T-UM-0.f editie) [PDF].

Drezner, T. D., & Drezner, Z. (2021). Informed cover measurement: Guidelines and error for point-intercept approaches. *Applications in Plant Sciences*, *9*(9–10). https://doi.org/10.1002/aps3.11446

Ding, W., Zvomuya, F., Cao, M., Wu, Y., & He, H. (2024). Ground cover management improves orchard soil moisture content–A global meta-analysis. *Journal of Hydrology*, 130710. https://doi.org/10.1016/j.jhydrol.2024.130710

Farrick, K. K., Wuddivira, M. N., & Martin, O. (2018). Estimation of soil texture from permanent wilting point measured with a chilled-mirror dewpoint technique. *Journal Of Plant Nutrition And Soil Science*, *182*(1), 119–125. https://doi.org/10.1002/jpln.201700573

Fitosoil Laboratorios, S.L. (2022). *Informe de ensayo: Análisis de suelo* (22060099.01).

Food and Agriculture Organization of the United Nations. (n.d.). *Key to the FAO Soil Units (1974)*. FAO. https://www.fao.org/soils-portal/data-hub/soil-classification/fao-legend/key-to-the-fao-soil-unit

García-Ruiz, J. M. (2010). The effects of land uses on soil erosion in Spain: A review. *CATENA*, *81*(1), 1–11. https://doi.org/10.1016/j.catena.2010.01.001

García-Ruiz, J. M., López-Moreno, J. I., Vicente-Serrano, S. M., Lasanta, T., & BegueríA, S. (2011). Mediterranean water resources in a global change scenario. *Earth-Science Reviews*, *105*(3–4), 121–139. https://doi.org/10.1016/j.earscirev.2011.01.006

Jeffers, A. ". (2019, February 11). *Soil texture Analysis "The Jar Test" | Home & Garden Information Center*. Home & Garden Information Center | Clemson University, South Carolina. https://hgic.clemson.edu/factsheet/soil-texture-analysis-the-jar-test/

Jeffers, A. ". (2023, December 1). *Soil texture Analysis "The Jar Test" | Home & Garden Information Center*. Home & Garden Information Center | Clemson University, South Carolina. https://hgic.clemson.edu/factsheet/soil-texture-analysis-the-jar-test/

Kirkham, M. (2005). Field Capacity, Wilting Point, Available Water, and the Non-Limiting Water Range. In *Elsevier eBooks* (pp. 101–115). https://doi.org/10.1016/b978-012409751-3/50008-6

Korres, W., Reichenau, T. G., Fiener, P., Koyama, C. N., Bogena, H., Cornelißen, T., Baatz, R., Herbst, M., Diekkrüger, B., Vereecken, H., & Schneider, K. (2015). Spatio-temporal soil moisture patterns – A meta-analysis using plot to catchment scale data. *Journal Of Hydrology*, *520*, 326–341. https://doi.org/10.1016/j.jhydrol.2014.11.042

Lehman, R. M., Cambardella, C. A., Stott, D. E., Acosta-Martínez, V., Manter, D. K., Buyer, J. S., Maul, J. E., Smith, J. L., Collins, H. P., Halvorson, J. J., Kremer, R. J., Lundgren, J. G., Ducey, T. F., Jin, V. L., & Karlen, D. L. (2015). Understanding and Enhancing Soil Biological Health: The Solution for Reversing Soil Degradation. *Sustainability*, *7*(1), 988–1027. https://doi.org/10.3390/su7010988

Lekshmi, S. S., Singh, D., & Baghini, M. S. (2014). A critical review of soil moisture measurement. *Measurement*, *54*, 92–105. https://doi.org/10.1016/j.measurement.2014.04.007

López-Vicente, M., Quijano, L., & Izquierdo, A. N. (2015). Spatial patterns and stability of topsoil water content in a rainfed fallow cereal field and Calcisol-type soil. *Agricultural Water Management*, *161*, 41–52. https://doi.org/10.1016/j.agwat.2015.07.009

MAPA, Ministerio de Agricultura (España). (2022). ECO-REGÍMENES EN CULTIVOS LEÑOSOS. In *mapa.gob.es* (GEN-9def-430b-9805-4f2c-493f-480e-0342-c116). Retrieved March 11, 2024, from https://www.mapa.gob.es/es/pac/pac-2023-2027/metodologia-calculo-importes-maximos-eco-regimenes-cultivos-lenosos_tcm30-626890.pdf

Mittelbach, H., Lehner, I., & Seneviratne, S. I. (2012). Comparison of four soil moisture sensor types under field conditions in Switzerland. *Journal Of Hydrology*, *430–431*, 39–49. https://doi.org/10.1016/j.jhydrol.2012.01.041

Prokopowicz, P., Pires, P. J. M., Michałek, A., Rybak, A., & Khairutdinov, A. M. (2020). Time necessary for microwave drying of mineral soils. *Journal Of Physics: Conference Series*, *1614*(1), 012021. https://doi.org/10.1088/1742-6596/1614/1/012021

Ramos, M., Benítez, E., GarcíA, P. G., & Robles, A. S. (2010). Cover crops under different managements vs. frequent tillage in almond orchards in semiarid conditions: Effects on soil quality. *Applied Soil Ecology*, *44*(1), 6–14. https://doi.org/10.1016/j.apsoil.2009.08.005

Ramsey, P. H. (1980). Exact Type 1 Error Rates for Robustness of Student's t Test with Unequal Variances. *Journal Of Educational Statistics*, *5*(4), 337–349. https://doi.org/10.3102/10769986005004337

Raya, A. M., Zuazo, V. H. D., & Martínez, J. R. F. (2005). Soil erosion and runoff response to plant-cover strips on semiarid slopes (SE Spain). *Land Degradation & Development*, *17*(1), 1–11. https://doi.org/10.1002/ldr.674

Ruíz-Colmenero, M., Bienes, R., & Marques, M. J. (2011). Soil and water conservation dilemmas associated with the use of green cover in steep vineyards. *Soil and Tillage Research*, *117*, 211–223. https://doi.org/10.1016/j.still.2011.10.004

Social i Company, R., & Gradziel, T. (2017). *Almonds: Botany, Production and Uses*. Cabi.

Soto, R. L., Padilla, M. C., & De Vente, J. (2020). Participatory selection of soil quality indicators for monitoring the impacts of regenerative agriculture on ecosystem services. *Ecosystem Services*, *45*, 101157. https://doi.org/10.1016/j.ecoser.2020.101157

TAFE Corporate. (2022, February). *Tillage - objectives & benefits*. TAFE. https://www.tafe.com/blog/tillage-objectives-benefits/

Talukder, R., Plaza-Bonilla, D., Cantero-Martínez, C., Di Prima, S., & Lampurlanés, J. (2022). Spatio-temporal variation of surface soil hydraulic properties under different tillage and maize-based crop sequences in a Mediterranean area. *Plant And Soil*. https://doi.org/10.1007/s11104-022-05758-x

Van Wesemael, B., Rambaud, X., Poesen, J., Muligan, M., Cammeraat, E., & Stevens, A. (2006). Spatial patterns of land degradation and their impacts on the water balance of rainfed treecrops: A case study in South East Spain. *Geoderma*, *133*(1–2), 43–56. https://doi.org/10.1016/j.geoderma.2006.03.036

Vereecken, H., Kamai, T., Harter, T., Kasteel, R., Hopmans, J. W., & Vanderborght, J. (2007). Explaining soil moisture variability as a function of mean soil moisture: A stochastic unsaturated flow perspective. *Geophysical Research Letters*, *34*(22). https://doi.org/10.1029/2007gl031813

Zhang, Z., & Peng, X. (2021). Bio-tillage: A new perspective for sustainable agriculture. *Soil And Tillage Research*, *206*, 104844. https://doi.org/10.1016/j.still.2020.104844

Zuazo, V. H. D., Pleguezuelo, C. R. R., Panadero, L. A., Raya, A. M., Martínez, J. R. F., & Rodríguez, B. C. (2009). Soil Conservation Measures in Rainfed Olive Orchards in South-Eastern Spain: Impacts of Plant Strips on Soil Water Dynamics. *Pedosphere*, *19*(4), 453–464. https://doi.org/10.1016/s1002-0160(09)60138-7

Zyserman, F., Monachesi, L. B., & Jouniaux, L. (2016). Dependence of shear wave seismoelectrics on soil textures: a numerical study in the vadose zone. *Geophysical Journal International*, *208*(2), 918–935. https://doi.org/10.1093/gji/ggw431

Supplements

Supplement A: Visual Soil Assessment

Results of the Visual Soil Assessment (Appendix A. of Soto et al., 2020) performed in the Shadow plot are displayed in Table S1. Considering a possible minimum and maximum score for questions nr. 8, 11, 12.1, and 13 the total score for the field's soil quality is between 29 and 39 which predominantly indicates a medium to high-quality soil (score range medium 26-37, high 38-48).

Question	**Topic**	**Score**	**Remarks**
1	Structure	1	See Figure S1
2.1	Organic matter - Colour	1	See Figure S1, see Fitosoil Laboratorios, S.L. (2022)
2.2	Organic matter - Odour	1	
3	Roots	1	Only sparsely in hardpan layer, see Figure S1
4	Worms	1	See Figure S1
5	Humidity	1	Measured with a 3-in-1 Soil meter, brand unknown, see Figure S2
6	Temperature	2 or 3	Measured with an Infrared Thermometer Surpeer IR5D Laser Values can differ e.g. on a hotter day
7	Vegetation cover	1	See Results Ground cover analysis
8	Ground cover vegetation colour	N.A.	[Not in Autumn]
9	Plant indicators	1	Almost only Tumbleweed, see Results Ground cover analysis
10	Erosion control	2 or 3	See Figure 12, and Figure 2
11	Infiltration capacity	N.D	No bigger rain event, therefore, no data
12.1	Yield - almond load and branch growth	N.A.	[Not in Autumn]
12.2	Yield - weight and size	1	200 kg/ha
13	Plant vigour	N.A.	[Not in Autumn]
14	Ladybugs	2	
	Total score	***29-39***	

Table S1. *Results of the Visual Soil Assessment performed in the Shadow plot.*

Figure S1. *Partly dug out soil located in the Shadow plot.*

Figure S2. *Humidity measurement in Shadow plot.*

Supplement B: Soil texture test

The results of the soil texture test were inconclusive, no separate layers were visible at any given moment in time (Figure S3). A repetition of the protocol with a taller jar gave the same inconclusive results. An existing lab report from a soil sample taken from the field (38°12'59.9"N 1°49'43.6"W) in 2022 unveiled the sand:silt:clay ratio to be 48%:28%:24% (Fitosoil Laboratorios, S.L., 2022). This indicates a loam soil texture, tending towards sandy clay loam (Figure S4). Equation 6 gave an estimated permanent wilting point of 17,5% in this loam soil.

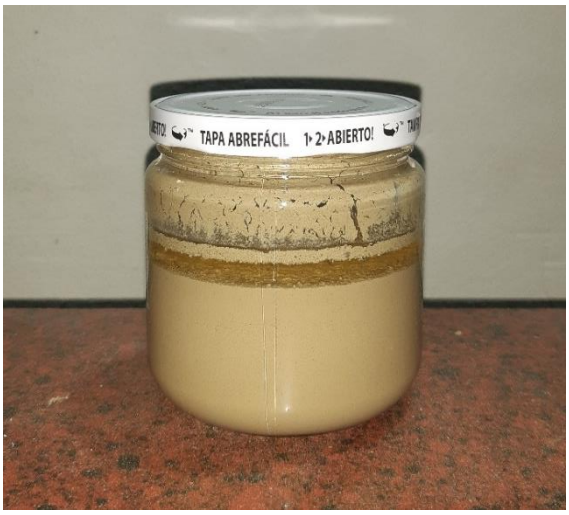

Figure S3. *Jar with soil sample, water, and detergent, 24 hours after mixing. Flash used.*

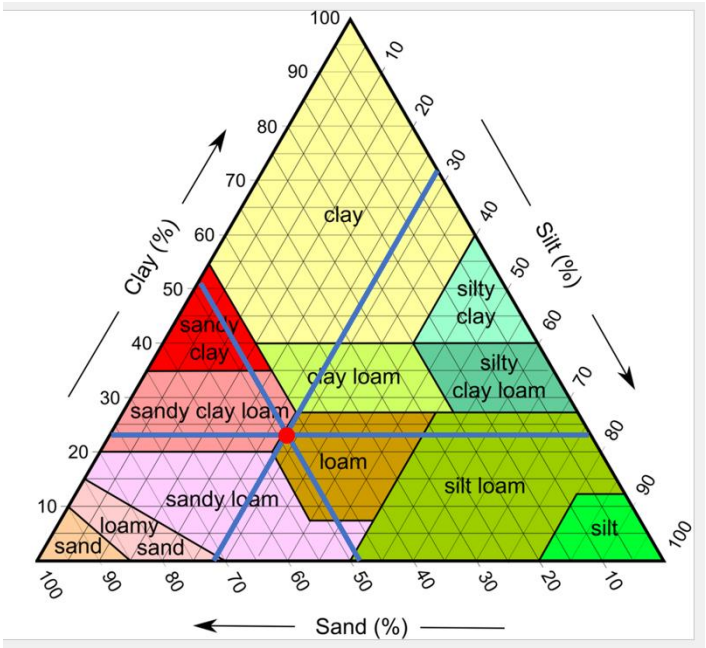

Figure S4. *Soil texture triangle indicating the loam soil texture type of the research field. Figure adapted from Zyserman et al. (2016) p. 923.*

Supplement C: Rainfall monitoring

Rainfall data obtained via the pluviometer at 38°13'12.0"N 1°49'06.5"W can be found in Table S2.

Rain events El Roble Autumn 2023		
date	**amount**	**unit**
20230911	1,5	L/m2
20230912	drops	
20230914	drops	
20230915	0,3	L/m2
20230916	1,8	L/m2
20230919	0,6	L/m2
20231015	drops	
20231016	drops	
20231023	0,1	L/m2
20231031	drops	

Start of topsoil moisture content measurements

Table S2. *Rainfall data monitored at 38°13'12.0"N 1°49'06.5"W using a pluviometer during the period 09-09-2023 till 17-12-2023.*